DIFFRACTION BY A PAIR OF IMPEDANCE HALF-PLANES AND AN IMPEDANCE HALF-PLANE

ON A GROUND PLANE

by

John L. Volakis
Radiation Laboratory
Department of Electrical Engineering and Computer Science
The University of Michigan
Ann Arbor, Michigan 48109

May 1985

388967-1-T = RL-2556

ABSTRACT

A rigorous solution is presented for the electromagnetic wave diffraction by (a) A pair of parallel perfectly conducting half planes, (b) A pair of parallel impedance half planes and (c) An impedance half plane in the presence of a ground plane. The above solutions are based on the angular spectrum method which is closely related to the Weiner-Hopf technique. In addition, a GTD solution is given which is valid when the separation distance between the half planes is large. Further, the diffraction of an impedance half plane in the presence of an impedance plane is considered in an approximate manner.

TABLE OF CONTENTS

I. INTRODUCTION

This report describes the solution to the high frequency plane wave diffraction by the four structures illustrated in Fig. 1. These are

(a) Two parallel perfectly conducting half planes.

(b) Two parallel impedance half planes.

(c) An impedance half-plane over a perfectly conducting plane.

(d) An impedance half plane over an impedance plane.

The problem of diffraction by the geometry in Fig. 1(a) was first considered by Heins [1,2] via the traditional Weiner Hopf technique and later by Clemmow [3] via the angular spectrum method. It should be emphasized that the two approaches of analysis are basically equivalent. Usually a solution performed with one method can also be completed with the other. Because of the relative conciseness of the angular spectrum method, this will be employed in our diffraction analysis of the subsequent geometries in Figs. 1(b) through 1(d). Since this analysis is intended for use in the study of diffraction by a thick impedance half plane, the boundary conditions in the inner face of the half planes is not considered. A GTD (geometrical theory of diffraction) solution is also given for all of the configurations in Fig. 1. The GTD solution is generally applicable for $\ell > \lambda/4$, where 2ℓ is the separation distance of the half plane and λ is the wavelength.

The solution to the problem of diffraction by the two parallel half planes requires a generalization of the angular spectrum method to include the existence of electric and magnetic currents on the impedance half planes. The generated integral equations in terms of the spectral density functions of these currents are ultimately decoupled
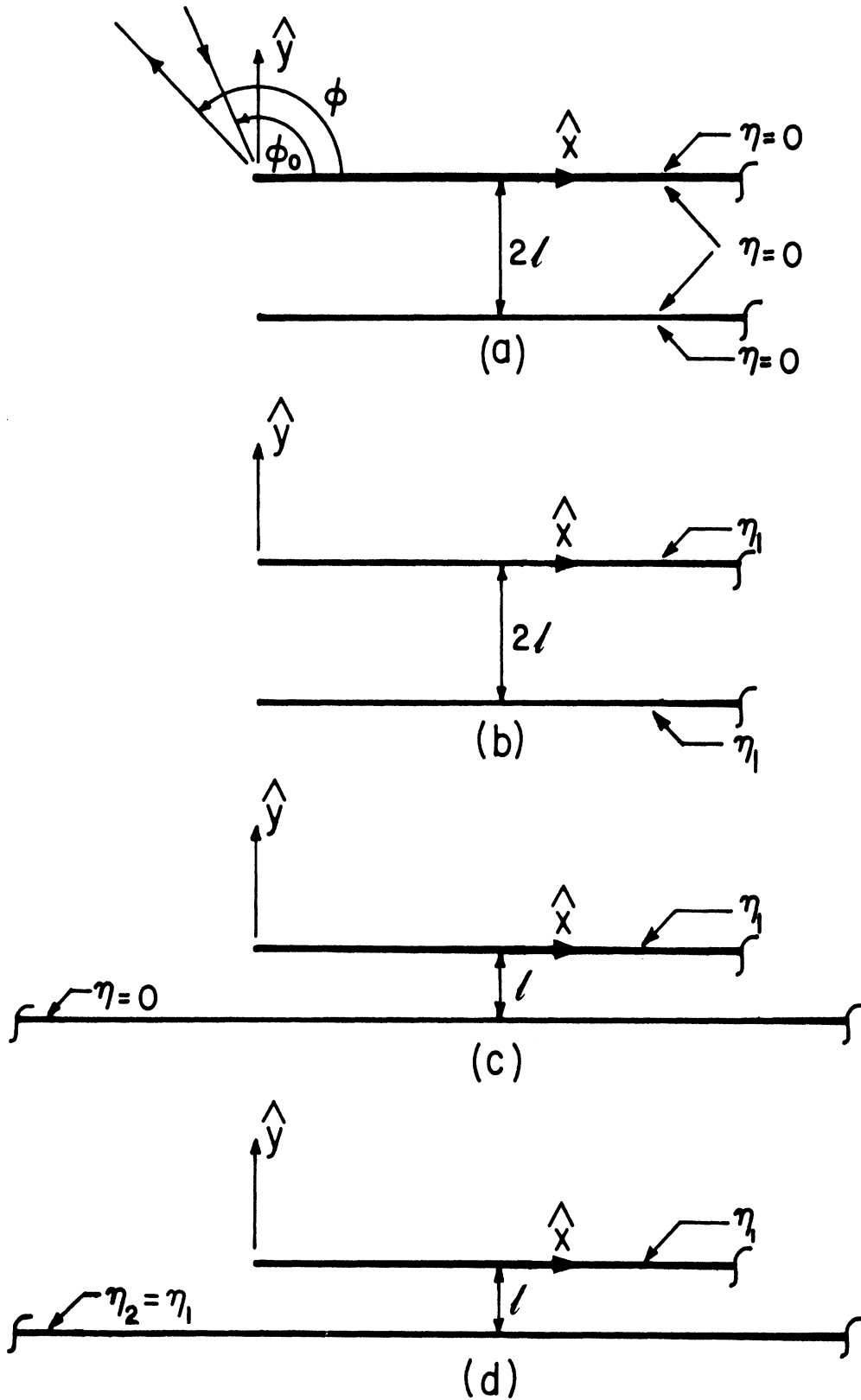
Figure 1. Geometry of the four structures under study
(η_1 denotes the normalized surface impedance).

on the basis that the magnetic currents vanish when the surface impedance is zero. A GTD solution to this configuration is rather simple provided the diffraction coefficient for the impedance half plane is incorporated in the corresponding GTD solution for the parallel perfectly conducting half planes.

Once the diffracted fields by the geometry in Fig. 1(b) has been obtained, one can then tackle the configurations in Figs. 1(c) and 1(d) by invoking image theory. Clearly, the diffracted field by the geometry in Fig. 1(c) with the perfectly conducting half plane can be obtained rigorously. However, the diffracted field by the geometry in Fig. 1(d) which includes an impedance plane can only be evaluated approximately at this time.

The report contains five chapters. Chapter II presents the formal solution of the diffracted field via the angular spectrum method. Although the E_z solution has already been given by Clemmow [3], this chapter serves the purpose of introducing the method of analysis and in addition presents the solution for the H_z incidence not completed by Clemmow.

Chapter III considers the diffraction by two parallel impedance half planes.

Chapter IV employs the results of Chapter III to formulate solutions for the diffracted field by an impedance half plane parallel to a ground plane or an impedance plane.

Finally, Chapter V discusses the approach to be used in incorporating the above analysis for the diffraction by a step discontinuity or protrusion on a ground or impedance plane.

II. DIFFRACTION BY A PAIR OF PARALLEL PERFECTLY CONDUCTING HALF PLANES

2.1 Introduction

As discussed in the introduction, the electromagnetic problem of a pair of perfectly conducting, half planes has been considered by a number of investigators. First Heins etc [1,2] obtained a Wiener-Hopf solution to the problems of reflection and coupling due to a plane wave incidence. However, a study on the diffraction pattern was not performed. Nevertheless, the difficult task of obtaining the required split functions was accomplished. Clemmow [3] later used the angular spectrum method [4] to obtain a solution for the diffraction by a pair of parallel half planes. His solution again involves the split functions obtained by Heins but is less involved because it avoids the direct computation of the currents on the half planes. Clemmow gives the scattering solution for the soft case (TM) only. However his method is applicable to the hard case (TE) as well. This is indeed accomplished in this chapter.

Lee and Mittra [5] generalized Heins hard case solution (see also Noble [6]) to include the effects of a recessed stub between the parallel half planes. They also appear to be the only authors to date who have published computed results for the scattering by a pair of perfectly conducting half planes and a thick edge (stub has zero recession).

Thus the solution of the diffraction by a pair of perfectly conducting half planes can be found in the literature. However,

these exist in various forms and are in some cases incomplete for our use. It is therefore instructive to rederive the scattering solutions from a pair of perfectly conducting half planes using a consistent method and approach suitable to our needs. In doing this we need to choose a method which can be extended to the scattering solution of the same geometry when it is associated with impedance boundary conditions representing a thin material coating. Clemmow's angular spectrum method was found to give promising results in this direction as it will be examined later.

The angular spectrum method involves the representation of the scattered field by an integral of plane waves. The weighting coefficients corresponding to these plane waves are referred to as the angular (continuous) spectra of the scattered field and are proportional to the surface currents via a Fourier integral transform. A solution to the scattered field then involves the determination of this angular spectrum after invoking the required boundary conditions and certain continuity conditions. Subsequently, the scattered or diffracted field is obtained via an asymptotic evaluation of the integral such as the steepest descent path method.

For the perfectly conducting pair of half planes considered in this section, only electric currents exist on the planar surfaces and thus a single angular spectrum on each half plane is required. However, in the next section, where the pair of impedance half planes is considered, both electric and magnetic angular spectra on each half plane must be included in the solution.

2.2 H_z-Incidence

Consider a plane wave (an $e^{j\omega t}$ factor is assumed and suppressed throughout)

$$H_z^i = e^{jk(x \cos \phi_0 + y \sin \phi_0)} \tag{1}$$

to be incident on the perfectly conducting geometry in Fig. 1(a). Employing now the angular spectrum method, the scattered H-field can be represented in terms of its angular spectrum as

$$H_z^{sa} = \pm \int_C [P_1(\cos \alpha) + P_2(\cos \alpha)e^{-j2k\ell \sin \alpha}]e^{-jkr \cos(\phi \mp \alpha)}d\alpha; \quad y \begin{array}{c} \geq 0 \\ \leq -2\ell \end{array} \tag{2}$$

where C is the contour shown in Fig. 2, $P_1(\cos \alpha)$ is associated with the upper half plane and $P_2(\cos \alpha)$ with the lower one. If we define

$$\lambda = \cos \alpha , \tag{3}$$

it is clear that in the λ-plane the C contour traverses from $-\infty$ to ∞ and it is indented at $\lambda = -1$, $-\lambda_0$, 1 as illustrated (note $\lambda_0 = \cos \phi_0$). In the α-plane this path corresponds to that for which $\cos \alpha$ remains real. The following outlines a procedure for finding $P_1(\cos \alpha)$ and $P_2(\cos \alpha)$.

According to (2), the scattered field component E_x^{sa} is given by

$$E_x^{sa} = -Z_0 \int_C \sin \alpha \left[P_1(\cos \alpha) + P_2(\cos \alpha)e^{+jk\ell \sin \alpha} \right] e^{-jkr \cos(\phi \mp \alpha)}d\alpha;$$

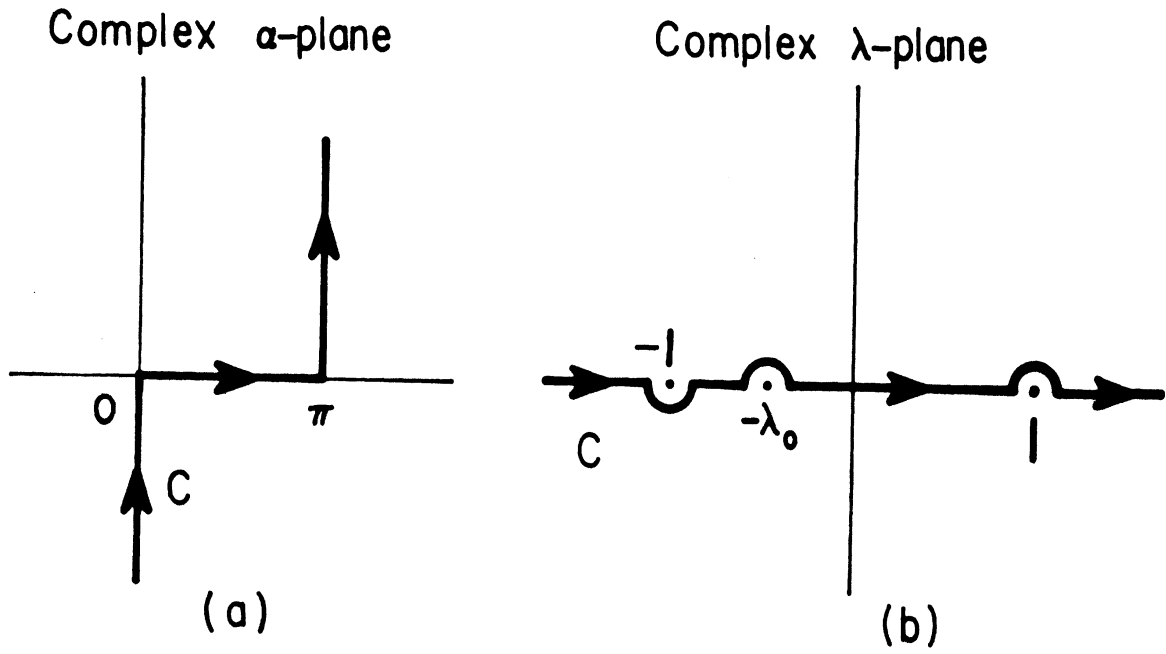$$y \begin{array}{c} \geq 0 \\ \leq -2\ell \end{array} \tag{4}$$

Figure 2. Illustration of the C contour in the α and λ complex planes.

where Z_0 is the free space impedance. The boundary condition $E_x^{sa} + E_x^i = 0$ on the surfaces $y = 0$, $x > 0$ and $y = -2\ell$, $x > 0$ require the solution of the following integral equations for $x > 0$,

$$\int_{-\infty}^{\infty} [P_1(\lambda) + P_2(\lambda)e^{-2jk\ell\sqrt{1-\lambda^2}}] \, e^{-jkx\lambda} \, d\lambda = \sqrt{1 - \lambda_0^2} \, e^{jkx\lambda_0} \tag{5a}$$

and

$$\int_{-\infty}^{\infty} [P_1(\lambda)e^{-2jk\ell\sqrt{1-\lambda^2}} + P_2(\lambda)]e^{-jkx\lambda} \, d\lambda = \sqrt{1 - \lambda_0^2} \, e^{-j2k\ell\sqrt{1-\lambda^2}} \, e^{jkx\lambda_0} . \tag{5b}$$

The above were obtained by noting that

$$E_x^i = \sin \phi_0 \, e^{jk(x \cos \phi_0 + y \sin \phi_0)} \tag{6}$$

and

$$d\lambda = \sin \alpha \, d\alpha . \tag{7}$$

In addition, field continuity over the planes $y = 0$, $x < 0$ and $y = -2\ell$, $x < 0$, requires that H_z^{sa} be continuous across these boundaries. From (2) this condition gives

$$\int_{-\infty}^{\infty} \left[\frac{P_1(\lambda)}{\sqrt{1 - \lambda^2}} + \frac{P_2(\lambda)}{\sqrt{1 - \lambda^2}} e^{-j2k\ell\sqrt{1-\lambda^2}} \right] e^{-jkx\lambda} \, d\lambda = 0 \tag{8a}$$

$$\int_{-\infty}^{\infty} \left[\frac{P_1(\lambda)}{\sqrt{1 - \lambda^2}} e^{-j2k\ell\sqrt{1-\lambda^2}} + \frac{P_2(\lambda)}{\sqrt{1 - \lambda^2}} \right] e^{-jkx\lambda} \, d\lambda = 0 \tag{8b}$$

for x < 0.   After closing the integration paths by a semi-infinite path in the upper half plane, it is clear that the above are satisfied only if $P_1(\lambda)/\sqrt{1 - \lambda^2}$ and $P_2(\lambda)/\sqrt{1 - \lambda^2}$ are free of singularities and zeros (i.e., regular) in the upper λ half plane. This is the region above the contour on the real axis shown in Fig. 2.   Denoting such functions as U-functions and those having the same properties in the lower half plane as L-functions, we conclude that

$$P_1(\lambda) = \sqrt{1 + \lambda}\ U_{1h}(\lambda) \tag{9a}$$

and

$$P_2(\lambda) = \sqrt{1 + \lambda}\ U_{2h}(\lambda)\ . \tag{9b}$$

$U_{1h}(\lambda)$ and $U_{2h}(\lambda)$ are now regular in the upper half plane and such a notation will be employed throughout this report.   Note also that the factor $\sqrt{1 + \lambda}$ is regular in the lower half plane and $\sqrt{1 - \lambda}$ is regular in the upper half plane.   Thus, if we write $\sqrt{1 - \lambda^2} = \sqrt{1 - \lambda}\ \sqrt{1 + \lambda}$ and use (9), it is clear that the terms $P_{1,2}(\lambda)/\sqrt{1 - \lambda^2}$ in (8) are regular in the upper half plane.

In order to find expressions for $P_{1,2}(\lambda)$ according to (5) and in view of (9), we first proceed to write (5) in a more convenient form. By adding and subtracting (5a) and (5b) we obtain the equivalent integral equations

$$\int_{-\infty}^{\infty} \sqrt{1 + \lambda}\ Q_1(\lambda)\ (1 + e^{-j2k\ell\sqrt{1-\lambda^2}})e^{-jkx\lambda}\ d\lambda = \sqrt{1 - \lambda_o^2}$$

$$\cdot (1 + e^{-j2k\ell\sqrt{1-\lambda_o^2}})e^{jkx\lambda_o} \tag{10a}$$

and

$$\int_{-\infty}^{\infty} \sqrt{1 + \lambda}\ Q_2(\lambda)\ (1 - e^{-2jk\ell\sqrt{1-\lambda^2}})e^{-jkx\lambda}\ d\lambda\ =\ \sqrt{1 - \lambda_0^2}\ (1 - e^{-2jk\ell\sqrt{1-\lambda_0^2}})e^{jkx\lambda_0}$$

(10b)

for x > 0, where

$$Q_{1,2}(\lambda)\ =\ U_{1h}(\lambda) \pm U_{2h}(\lambda)\ .$$

(11)

By defining the branch of $\sqrt{1 - \lambda^2}$ to always have a negative imaginary part we then close the path of integration in (10) by a semi-circular contour at infinity of the lower λ half plane. Subsequently, employing Cauchy's theorem, we find that

$$\sqrt{1 + \lambda}\ Q_1(\lambda)(1 + e^{-j2k\ell\sqrt{1-\lambda^2}})\ =\ -\frac{\sqrt{1 - \lambda_0^2}}{2\pi j}\ (1 + e^{-j2k\ell\sqrt{1-\lambda_0^2}})$$

$$\cdot \frac{L_{1h}(\lambda)}{L_{1h}(-\lambda_0)}\ \frac{1}{\lambda + \lambda_0}$$

(12a)

and

$$\sqrt{1 + \lambda}\ Q_2(\lambda)(1 - e^{-j2k\ell\sqrt{1-\lambda^2}})\ =\ -\frac{\sqrt{1 - \lambda_0^2}}{2\pi j}\ (1 - e^{-j2k\ell\sqrt{1-\lambda_0^2}})$$

$$\cdot \frac{L_{2h}(\lambda)}{L_{2h}(-\lambda_0)}\ \frac{1}{\lambda + \lambda_0}\ .$$

(12b)

As we mentioned earlier the $L_{1h}(\lambda)$, $L_{2h}(\lambda)$ functions are regular in the lower half plane. The ratio of $L(\lambda)/L(-\lambda_0)$ is clearly equal to unit at the pole $\lambda = -\lambda_0$ so that the residue of this pole gives the result in the right hand side of (10).

A solution to $Q_{1,2}(\lambda)$ requires first the factorization of the expressions $(1 \pm e^{-j2k\ell\sqrt{1-\lambda^2}})$ in terms of U and L functions. This has been accomplished by Heins [1,2] with the $e^{-j\omega t}$ time convention and have been used by Clemmow [3] and Lee and Mittra [5] in certain calculations. We simply quote here that

$$1 + e^{-j2k\ell\sqrt{1-\lambda^2}} = U_1(\lambda)L_1(\lambda) \tag{13a}$$

and

$$1 - e^{-j2k\ell\sqrt{1-\lambda^2}} = U_2(\lambda)L_2(\lambda) \quad . \tag{13b}$$

The split functions $U_{1,2}(\lambda) = L_{1,2}(-\lambda)$ are regular in the upper half plane and their holomorphic expressions are given in Appendix I according to the $e^{j\omega t}$ time convention employed here. Simplified expressions suitable for small ℓ are also given in Appendix I.

From (12) and (13), and since $Q_{1,2}(\lambda)$ are U-functions we find that

$$Q_1(\lambda) = -\frac{1}{2\pi j} \frac{L_1(\lambda_0)\ \sqrt{1+\lambda_0}}{U_1(\lambda)(\lambda + \lambda_0)} \tag{14a}$$

and

$$Q_2(\lambda) = -\frac{1}{2\pi j} \frac{L_2(\lambda_0)\sqrt{1+\lambda_0}}{U_2(\lambda)(\lambda + \lambda_0)} \tag{14b}$$

In addition,

$$L_{1h}(\lambda) = \sqrt{1+\lambda}\ L_1(\lambda) \quad , \tag{15}$$

and

$$L_{1h\atop 2h}(-\lambda_0) = \sqrt{1 - \lambda_0} \; L_1(-\lambda_0) = \sqrt{1 - \lambda_0} \; U_1(\lambda_0) \quad . \quad (16)$$

Finally, from (9), (11), (14) and (3) we find that the angular spectra associated with the upper and lower perfectly conducting half planes are given by

$$P_{1\atop 2}(\cos \phi) = -\frac{1}{4\pi j} \frac{2 \cos \phi/2 \cos \phi_0/2}{\cos \phi + \cos \phi_0} \left[\frac{L_1(\cos \phi_0)}{U_1(\cos \phi)} \pm \frac{L_2(\cos \phi_0)}{U_2(\cos \phi)} \right] .$$

$$(17)$$

Using (17) in (2) and evaluating the integral via the steepest descent method it is obtained that the scattered field is

$$H_z^{sa} = \sqrt{\frac{2\pi}{kr}} \; [P_1(\cos \phi) + P_2(\cos \phi)e^{-j2k\ell \sin \phi}]e^{-jkr}e^{j\pi/4};$$

$$(18)$$

or

$$H_z^{sa} = \left[-\frac{1}{\sqrt{2\pi k}} e^{-j\pi/4} \frac{2 \cos \phi/2 \cos \phi_0/2}{\cos \phi + \cos \phi_0} \right] e^{-jk\ell \sin \phi}$$

$$\cdot \left[\frac{L_1(\cos \phi_0)}{U_1(\cos \phi)} \cos(k\ell \sin \phi) + j \frac{L_2(\cos \phi_0)}{U_2(\cos \phi)} \sin(k\ell \sin \phi) \right] \frac{e^{-jkr}}{\sqrt{r}} \; ;$$

$$(19)$$

Noting that the factor

$$D_h(\phi,\phi_0) = -\frac{e^{-j\pi/4}}{\sqrt{2\pi k}} \frac{2 \cos \phi/2 \cos \phi_0/2}{\cos \phi + \cos \phi_0} \qquad (20)$$

is the hard diffraction coefficient for the edge of a perfectly

conducting half plane we may express H_z^{sa} more compactly as

$$H_z^{sa} = D_h(\phi,\phi_0)\Delta(\phi,\phi_0;\ell)\frac{e^{-jkr}}{\sqrt{r}} \; ; \tag{21}$$

where

$$\Delta(\phi,\phi_0;\ell) = e^{-jk\ell \sin \phi} \left[\frac{L_1(\cos \phi_0)}{U_1(\cos \phi)} \cos(k\ell \sin \phi) + j \frac{L_2(\cos \phi_0)}{U_2(\cos \phi)} \right.$$
$$\left. \cdot \sin(k\ell \sin \phi) \right] . \tag{22}$$

It will be clear in the later sections that $\Delta(\phi,\phi_0,\ell)$ is a geometry

dependent factor and corresponds to the interactions between the two

half planes. In addition, although not obvious from (22), it can be

proven with the use of (13) that (21) satisfies reciprocity as required.

Since for $\ell = 0$ (see Appendix I or Eq. (13)),

$$L_1(\cos \phi) = U_1(\cos \phi) = \sqrt{2}$$

it follows that

$$\Delta(\phi,\phi_0;0) = 1$$

and thus (23) reduces to the diffracted field by a perfectly conducting

half plane as required. Further, because $D_h(\pi,\pi) = 0$, H_z^{sa} vanishes

when $\phi = \phi_0 = \pi$, i.e., at grazing.

2.3 E_z-Incidence

The analysis for finding the scattered field with a plane wave

$$E_z^i = e^{+jk(x \cos \phi_0 + y \sin \phi_0)} \tag{23}$$

incident onto the geometry of Fig. 1(a) is similar to that presented

for the H_z (TE) case.

In terms of its angular spectrum, the scattered E-field can be

represented as

$$E_z^{sa} = \int_C [P_1(\cos \alpha) + P_2(\cos \alpha)e^{-j2k\ell \sin \alpha}] e^{-jkr \cos(\phi \mp \alpha)} d\alpha; \quad y \gtrless -2\ell \tag{24}$$

and the solution reduces to finding $P_{1,2}(\cos \phi)$ as before. The

boundary condition $E_z^s + E_z^i = 0$ requires that

$$\int_{-\infty}^{\infty} \left[\frac{P_1(\lambda)}{\sqrt{1 - \lambda^2}} + \frac{P_2(\lambda)}{\sqrt{1 - \lambda^2}} e^{-j2k\ell\sqrt{1-\lambda^2}} \right] e^{-jkx\lambda} d\lambda = -e^{jkx\lambda_0} \tag{25a}$$

and

$$\int_{-\infty}^{\infty} \left[\frac{P_1(\lambda)}{\sqrt{1 - \lambda^2}} e^{-j2k\ell\sqrt{1-\lambda^2}} + \frac{P_2(\lambda)}{\sqrt{1 - \lambda^2}} \right] e^{-jkx\lambda} d\lambda = -e^{jkx\lambda_0} e^{-j2k\ell\sqrt{1-\lambda_0^2}} \tag{25b}$$

for x > 0. In addition, continuity of the tangential H-field (H_x) over

the region x < 0 requires that

$$\int_{-\infty}^{\infty} [P_1(\lambda) + P_2(\lambda) e^{-j2k\ell\sqrt{1-\lambda^2}}] e^{-jkx\lambda} d\lambda = 0 \tag{26a}$$

and

$$\int_{-\infty}^{\infty} [P_1(\lambda)e^{-j2k\ell\sqrt{1-\lambda^2}} + P_2(\lambda)] \, e^{-jkx\lambda} \, d\lambda = 0 \qquad (26b)$$

for x < 0. Alternatively, (26) could be formulated by noting that electric currents scatter zero tangential H-field in the planes which contain them.

Equation (26) clearly implies that $P_{1,2}(\lambda)$ are U-functions, i.e., regular in the upper λ-half plane shown in Fig. 2. Therefore,

$$P_1(\lambda) = U_{1e}(\lambda) \qquad (27)$$
$$ \, {}_2 {}_{2e}$$

Similarly to the H_z case, we also find by adding and subtracting (25) and subsequently employing Cauchy's theorem, that

$$\frac{Q_1(\lambda)}{\sqrt{1-\lambda^2}} (1 + e^{-j2k\ell\sqrt{1-\lambda^2}}) = \frac{1}{2\pi j} (1 + e^{-j2k\ell\sqrt{1-\lambda^2}}) \frac{L_{1e}(\lambda)}{L_{1e}(-\lambda_0)} \frac{1}{\lambda + \lambda_0} \qquad (28a)$$

and

$$\frac{Q_2(\lambda)}{\sqrt{1-\lambda^2}} (1 - e^{-2jk\ell\sqrt{1-\lambda^2}}) = \frac{1}{2\pi j} (1 - e^{-j2k\ell\sqrt{1-\lambda^2}}) \frac{L_{2e}(\lambda)}{L_{2e}(-\lambda_0)} \frac{1}{\lambda + \lambda_0} \qquad (28b)$$

where $Q_1(\lambda) = P_1(\lambda) + P_2(\lambda) = U_{1e}(\lambda) + U_{2e}(\lambda)$ \qquad (29a)

and

$$Q_2(\lambda) = P_1(\lambda) - P_2(\lambda) = U_{1e}(\lambda) - U_{2e}(\lambda) \ . \qquad (29b)$$

In view of (13) and (29), equations (28) are satisfied by

$$Q_1(\lambda) = \frac{1}{2\pi j} \frac{L_1(\lambda_0)}{U_1(\lambda)} \frac{\sqrt{1-\lambda}\,\sqrt{1-\lambda_0}}{\lambda + \lambda_0} \tag{30a}$$

and

$$Q_2(\lambda) = \frac{1}{2\pi j} \frac{L_2(\lambda_0)}{U_2(\lambda)} \frac{\sqrt{1-\lambda}\,\sqrt{1-\lambda_0}}{\lambda + \lambda_0} \ . \tag{30b}$$

The split functions $U_{1,2}(\lambda) = L_{1,2}(-\lambda)$ are discussed in Appendix I.

From (29) we obtain that

$$P_{\substack{1 \\ 2}}(\cos \phi) = \frac{1}{4\pi j} \frac{2 \sin \phi/2 \sin \phi_0/2}{\cos \phi + \cos \phi_0} \left[\frac{L_1(\cos \phi_0)}{U_1(\cos \phi)} \pm \frac{L_2(\cos \phi_0)}{U_2(\cos \phi)} \right] \ . \tag{31}$$

Substitution in (24) and subsequent evaluation of the integral via the steepest descent method gives

$$E_z^{sa} = D_s(\phi,\phi_0)\Delta(\phi,\phi_0;\ell) \frac{e^{-jkr}}{\sqrt{r}} \ . \tag{32}$$

As expected, $D_s(\phi,\phi_0)$ is now the soft diffraction coefficient associated with the diffraction by the edge of a perfectly conducting half plane. Specifically

$$D_s(\phi,\phi_0) = \frac{e^{-j\pi/4}}{\sqrt{2\pi k}} \frac{2 \sin \phi/2 \sin \phi_0/2}{\cos \phi + \cos \phi_0} \tag{33}$$

The geometry function $\Delta(\phi,\phi_0;\ell)$ is the same as in the H_z incidence and is given in (22).

2.4 A GTD Solution for Large ℓ

When $\ell > \lambda/4$, a solution for the diffraction by the geometry in Fig. 1(a) in the context of the geometrical theory of diffraction (GTD) [7] may be applicable. This process requires the summation of the contributions from all six ray mechanisms illustrated in Fig. 3. Using the asymptotic expansion of Bowman [8] for large $k\ell$, we find that to the $O(1/k\ell)$,

$$\left.\begin{array}{c}E_{z_1}^a\\[4pt]H_{z_1}^a\end{array}\right\} = u_z^1 = D_{\substack{s\\h}}(\phi,\phi_0)\,\frac{e^{-jkr}}{\sqrt{r}} \tag{34a}$$

$$u_z^2 = D_{\substack{s\\h}}(\phi,\phi_0)e^{-j2k\ell(\sin\phi + \sin\phi_0)}\,\frac{e^{-jkr}}{\sqrt{r}}\,, \tag{34b}$$

$$u_z^{12} = \frac{e^{-j\pi/4}}{\sqrt{4\pi k\ell}}\left(\frac{1}{\cos\phi} + \frac{1}{\cos\phi_0}\right)D_{\substack{s\\h}}(\phi,\phi_0)e^{-j2k\ell\sin\phi_0}$$

$$\cdot\left(\sum_{m=0}^{\infty}\frac{e^{-j(2m+1)2k\ell}}{(2m+1)^{3/2}}\right)\frac{e^{-jkr}}{\sqrt{r}} \tag{34c}$$

$$u_z^{21} = \frac{e^{-j\pi/4}}{\sqrt{4\pi k\ell}}\left(\frac{1}{\cos\phi} + \frac{1}{\cos\phi_0}\right)D_{\substack{s\\h}}(\phi,\phi_0)e^{-2jk\ell\sin\phi}$$

$$\cdot\left(\sum_{m=0}^{\infty}\frac{e^{-j(2m+1)2k\ell}}{(2m+1)^{3/2}}\right)\frac{e^{-jkr}}{\sqrt{r}} \tag{34d}$$
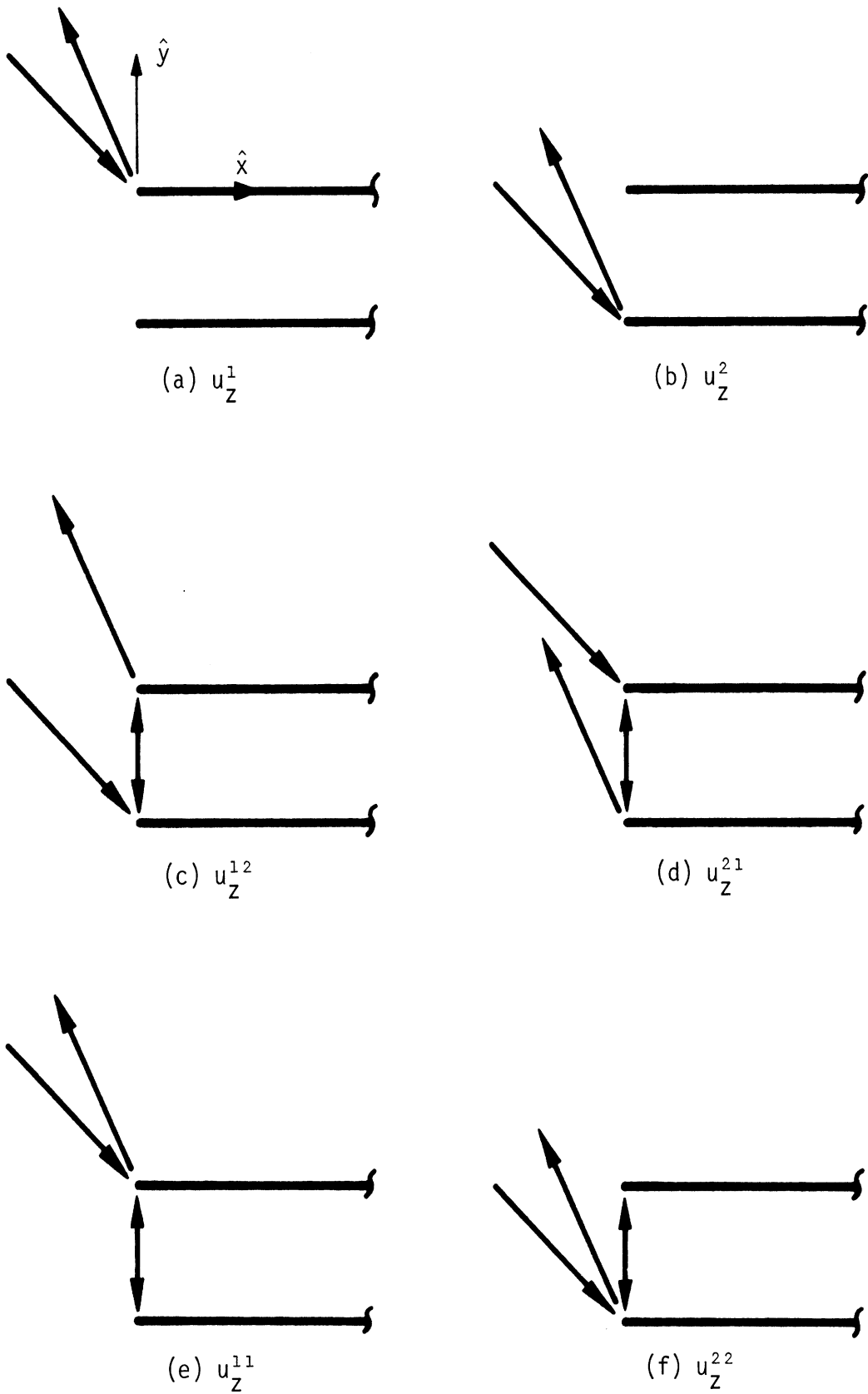
Figure 3. GTD interaction terms associated with two parallel half planes.

$$u_z^{11} = - \frac{e^{-j\pi/4}}{\sqrt{4\pi k\ell}} \left(\frac{1}{\cos \phi} + \frac{1}{\cos \phi_0} \right) D_{\substack{s\\h}}(\phi,\phi_0) \left(\sum_{m=1}^{\infty} \frac{e^{-j(2m)2k\ell}}{(2m)^{3/2}} \right) \frac{e^{-jkr}}{\sqrt{r}} \tag{34e}$$

and

$$u_z^{22} = - \frac{e^{-j\pi/4}}{\sqrt{4\pi k\ell}} \left(\frac{1}{\cos \phi} + \frac{1}{\cos \phi_0} \right) D_{\substack{s\\h}}(\phi,\phi_0) e^{-j2k\ell(\sin \phi + \sin \phi_0)}$$

$$\cdot \left(\sum_{m=1}^{\infty} \frac{e^{-j(2m)2k\ell}}{(2m)^{3/2}} \right) \frac{e^{-jkr}}{\sqrt{r}} \quad . \tag{34f}$$

In the above, u_z denotes components of either E_z^{sa} or H_z^{sa} corresponding to the sofe (D_s) or hard (D_h) diffraction coefficients, respectively. Furthermore, the infinite sums in 34(c) through (f) are associated with the multiple interactions between the upper and lower half plane edges as illustrated in Fig. 3(c) through (f). Each term in the m-series is divided by the factors $(2m + 1)^{3/2}$ or $(2m)^{3/2}$ and as seen from Table I, the first two to three terms are in most cases sufficient depending on the value of ℓ. More precisely, the number of terms needed for good accuracy is less for a larger separation distance between the half planes. In general,

$$\left. \begin{matrix} E_z^{sa} \\ \\ H_z^{sa} \end{matrix} \right\} \sim u_z^1 + u_z^2 + u_z^{12} + u_z^{21} + u_z^{11} + u_z^{22} \tag{35}$$

For relatively large ℓ, say 1.5 λ, the scattered field may even be approximated with only the singly diffracted fields from the upper and lower edges, viz for $\ell > 1.5 \lambda$

$$\left.\begin{array}{c} E_z^{sa} \\ \\ H_z^{sa} \end{array}\right\} \sim D_{\begin{subarray}{l}s\\h\end{subarray}}(\phi,\phi_0) \cos[k\ell(\sin \phi + \sin \phi_0)]e^{-jk\ell(\sin \phi + \sin \phi_0)} \frac{e^{-jkr}}{\sqrt{r}} \quad .$$

$$(36)$$

Table 2.1

Values of $(2m)^{3/2}$ and $(2m+1)^{3/2}$

m	$(2m)^{3/2}$	$(2m+1)^{3/2}$
0	--	1
1	2.83	5.2
2	8	11.18
3	14.7	18.5
4	22.63	27.0

III. DIFFRACTION BY A PAIR OF PARALLEL IMPEDANCE HALF PLANES

3.1 Introduction

The geometry relating to a pair of imperfectly conducting or impedance half planes is depicted in Fig. 1(b). An impedance (opaque) half plane is characterized by the boundary conditions

$$\bar{E} - (\hat{n} \cdot \bar{E})\hat{n} = \eta_1 Z_0 \hat{n} \times \bar{H} \tag{37}$$

on its upper and lower surfaces. $\bar{E}$ and $\bar{H}$ in (37) refer to the total fields and $\eta_1 = Z_s/Z_0$ is the normalized impedance on each face of the half plane. η_1 may also correspond to an equivalent surface impedance. For example, in case of a perfectly conducting half plane with a thin material coating on each of its faces, the problem is equivalent to an impedance half plane with

$$\eta_1 = j \tan k_d t \quad , \tag{38}$$

where t is the small thickness of the coating and k_d is the propagation constant associated with the material coating. In terms of the constitutive parameters

$$\mu_d = \mu_0 (\mu'_r - j\mu''_r) \quad , \tag{39a}$$

$$\varepsilon_d = \varepsilon_0 (\varepsilon'_r - j\varepsilon''_r) \tag{39b}$$

we have that

$$k_d = k_0 (k'_r - j k''_r) \tag{40a}$$

where

$$k_r' = K_{mr} \cos(\phi_d/2) \tag{40b}$$

$$k_r'' = K_{mr} \sin(\phi_d/2) \tag{40c}$$

$$K_{mr} = [(\mu_r'\varepsilon_r' - \varepsilon_r''\mu_r'')^2 + (\mu_r''\varepsilon_r' + \varepsilon_r''\mu_r')^2]^{1/4} \tag{40d}$$

and

$$\phi_d = \tan^{-1}\left[\frac{\mu_r''\varepsilon_r' + \varepsilon_r''\mu_r'}{\mu_r'\varepsilon_r' - \varepsilon_r''\mu_r''}\right] . \tag{40e}$$

Equation (38) may be even further approximated to give (for very small t) [9]

$$\eta_1 \approx jk_0 t \left(\frac{\mu_d}{\mu_0} - \frac{\varepsilon_0}{\varepsilon_d}\right) , \tag{41}$$

ε_0 and μ_0 are the free space permittivity and permeability.

The asymptotic solution to the diffraction by a single impedance half plane is given by Senior [10]. In addition, explicit (non-integral) uniform diffraction coefficients for the impedance half plane can be found in [11]. These will be used later in this section. However, the problem of diffraction by a pair of half planes shown in Fig. 1(b) has not been considered previoulsy. In the following we will develop such a solution. The approach of analysis will be based on the angular spectrum method and as such it will be a continuation or generalization of the procedure given in Section II. Once the scattering solutions to the problem in Fig. 1(b) has been developed it will serve as the basis for the diffraction by an impedance half-plane over a ground plane via image theory or, in an approximate manner, over an

impedance plane. Further the angular spectrum method can be used for obtaining the coupling into the parallel plate waveguide composed of a pair of impedance half planes. Subsequently, based on the above results the problem of diffraction or scattering by a coated protrusion can be considered.

3.2 Formulation of the Required Integral Equations

Because of the non-zero impedance on the half planes of Fig. 1(b), both electric and magnetic currents will exist on their surfaces. Therefore, the total scattered field will be given by

$$
\left.\begin{array}{c} E_z^s \\ H_z^s \end{array}\right\} = \left\{\begin{array}{c} E_z^{es} + E_z^{ms} \\ H_z^{es} + H_z^{ms} \end{array}\right. \tag{42}
$$

depending on the polarization of incidence under consideration. In (42), the components with the superscript es refer to the scattered field associated with the electric currents and those with the superscript ms refer to the scattered field associated with the magnetic currents.

According to the angular spectrum method, the scattered field components due to the configuration depicted in Fig. 1(b) may be respesented as follows (see also Chapter II):

In case of E_z incidence,

$$
E_z^{es} = \int_C [P_{1e}(\cos \alpha) + P_{2e}(\cos \alpha)e^{j2k\ell \sin \alpha}]e^{-jkr \cos(\phi \mp \alpha)} \, d\alpha \ ; \ y \begin{array}{c} \geq 0 \\ \leq -2\ell \end{array} \tag{43a}
$$

and

$$E_z^{ms} = \pm \int_C [P_{1m}(\cos \alpha) + P_{2m}(\cos \alpha)e^{2jk\ell \sin \alpha}]e^{-jkr \cos(\phi \mp \alpha)}d\alpha \; ; \; y \begin{array}{c} \geq 0 \\ \leq -2\ell \end{array}$$

$$(43b)$$

where C is the contour for which cos α remains real and is shown in Fig. 2. The corresponding H-fields are

$$H_x^{es} = \pm Y_0 \int_C \sin \alpha [P_{1e}(\cos \alpha) + P_{2e}(\cos \alpha)e^{2jk\ell \sin \alpha}]e^{-jkr \cos(\phi \mp \alpha)}d\alpha \; ;$$

$$y \begin{array}{c} \geq 0 \\ \leq -2\ell \end{array} \qquad (44a)$$

and

$$H_x^{ms} = Y_0 \int_C \sin \alpha [P_{1m}(\cos \alpha) + P_{2m}(\cos \alpha)e^{j2k\ell \sin \alpha}]e^{-jkr \cos(\phi \mp \alpha)}d\alpha \; ;$$

$$y \begin{array}{c} \geq 0 \\ \leq -2\ell \end{array} \qquad (44b)$$

In the above, $P_{1e}(\cos \alpha)$ and $P_{1m}(\cos \alpha)$ are the angular spectra associated with the top impedance half plane and similarly $P_{2e}(\cos \alpha)$ with $P_{2m}(\cos \alpha)$ correspond to the bottom half plane. Using the parameter $\lambda = \cos \alpha$, we further find that $P_{1e \atop 2e}(\lambda)$ correspond to the spectra of the electric currents, J_z, on the respective planes due to the discontinuity of H_x^{es}. Similarly, $P_{1m \atop 2m}(\alpha)/\sqrt{1 -\lambda^2}$ correspond to the spectra of the magnetic currents, M_x, due to the discontinuity of E_z^{ms} over the y = 0, x > 0 and y = -2ℓ, x < 0 planes.

In the case of H_z incidence, the scattered fields can be represented as

$$H_z^{es} = \pm \int_C [P_{1e}(\cos \alpha) + P_{2e}(\cos \alpha)e^{j2k\ell \sin \alpha}]e^{-jkr \cos(\phi \mp \alpha)}d\alpha \; ; \quad y \begin{array}{c} \geq 0 \\ \leq -2\ell \end{array}$$

(45a)

and

$$H_z^{ms} = + \int_C [P_{1m}(\cos \alpha) + P_{2m}(\cos \alpha)e^{j2k\ell \sin \alpha}]e^{-jkr \cos(\phi \mp \alpha)}d\alpha \; ; \quad y \begin{array}{c} \geq 0 \\ \leq -2\ell \end{array}$$

(45b)

The corresponding E-fields are

$$E_x^{es} = -Z_0 \int_C \sin \alpha [P_{1e}(\cos \alpha) + P_{2e}(\cos \alpha)e^{j2k\ell \sin \alpha}]e^{-jkr \cos(\phi \mp \alpha)}d\alpha \; ;$$

$$y \begin{array}{c} > 0 \\ < -2\ell \end{array}$$

(46a)

and

$$E_x^{ms} = \mp Z_0 \int_C \sin \alpha [P_{1m}(\cos \alpha) + P_{2m}(\cos \alpha)e^{j2k\ell \sin \alpha}]e^{-jkr \cos(\phi \mp \alpha)}d\alpha \; ;$$

$$y \begin{array}{c} > 0 \\ < -2\ell \end{array} \cdot$$

(46b)

The determination of the above spectra $P_{\substack{1e \\ 2e}}(\lambda)$ and $P_{\substack{1m \\ 2m}}(\lambda)$ requires the simultaneous solution of an equal number of integral equations. These can be obtained by imposing the necessary continuity and boundary conditions. For brevity purposes, below we discuss the construction of the required integral equations for the E_z incidence only. The corresponding equations for the H_z-incidence can be obtained in a similar manner on the basis of Eqs (45) and (46).

For the E_z-incidence a set of integral equations can be obtained if we note that H_x^{es} vanishes in the plane of the electric current sheets and via duality E_z^{ms} also vanishes in the plane of the magnetic current sheet. These conditions require that

$$\int_{-\infty}^{\infty} P_{1e}(\lambda)\, e^{-jkx\lambda}\, d\lambda \;=\; 0 \text{ for } \quad x < 0 \;, \qquad (47a)$$

$$\int_{-\infty}^{\infty} P_{2e}(\lambda)e^{-jkx\lambda}\, d\lambda \;=\; 0 \quad \text{ for } x < 0 \;, \qquad (47b)$$

$$\int_{-\infty}^{\infty} \frac{P_{1m}(\lambda)}{\sqrt{1 - \lambda^2}}\, e^{-jkx\lambda}\, d\lambda \;=\; 0 \quad \text{ for } x < 0 \;, \qquad (47c)$$

and

$$\int_{-\infty}^{\infty} \frac{P_{2m}(\lambda)}{\sqrt{1 - \lambda^2}}\, e^{-jkx\lambda}\, d\lambda \;=\; 0 \quad \text{ for } x < 0 \;. \qquad (47d)$$

Equations (47) are similar to Eqs. (8) and (26) in Chapter II and imply that

$$P_{\substack{1e \\ 2e}}(\lambda) \;=\; U_{\substack{1e \\ 2e}}(\lambda) \qquad (48a)$$

and

$$P_{\substack{1m \\ 2m}}(\lambda) \;=\; \sqrt{1 + \lambda}\; U_{\substack{1m \\ 2m}}(\lambda) \;. \qquad (48b)$$

As before, the U-functions refer to regular functions in the upper λ-half plane.

Additional integral equations can be obtained by imposing the impedance boundary condition (see Eq. (37)),

$$(E_z^s + E_z^i) \;=\; -\eta_1 Z_0 (H_x^s + H_x^i) \qquad (49)$$

on the outer faces of the top and bottom half planes. The boundary conditions on the inner faces of the half planes are not considered at this time since the ultimate use of this analysis is the study of a thick impedance half plane.

Substitution of Eqs. (42) through (44) into (49) requires on both outer

faces of the impedance half planes that

$$\int_{-\infty}^{\infty} \left(\frac{1}{\sqrt{1-\lambda^2}} + \eta_1\right) \left\{[P_{1e}(\lambda) + P_{1m}(\lambda)] + [P_{2e}(\lambda) + P_{2m}(\lambda)]e^{-j2k\ell\sqrt{1-\lambda^2}}\right\} e^{-jkx\lambda} d\lambda$$

$$= -(1 - \eta_1\sqrt{1 - \lambda_0^2})\, e^{jkx\lambda_0} \qquad (50a)$$

and

$$\int_{-\infty}^{\infty} \left(\frac{1}{\sqrt{1-\lambda^2}} + \eta_1\right) \left\{[P_{1e}(\lambda) - P_{1m}(\lambda)]e^{-j2k\ell\sqrt{1-\lambda^2}} + [P_{2e}(\lambda) - P_{2m}(\lambda)]\right\} e^{-jkx\lambda} d\lambda$$

$$= -(1 - \eta\sqrt{1 - \lambda_0^2})e^{jkx\lambda_0}\, e^{-j2k\ell\sqrt{1-\lambda^2}}$$

for $x > 0$. Provided the boundary conditions in the inner faces of the half

planes are of no interest, equations (50) along with (48) are sufficient

for determining $P_{1e}(\lambda)$ and $P_{1m}(\lambda)$. Their solution is presented in the
${}_{2m}$
next section.

3.3 E_z Incidence

In this section the solution of equations (50) in view of (48)

is outlined. Similarly to the development in Chapter II, once the

angular spectra are determined, it is then a trivial task for obtaining

the scattered field. We proceed now to solve Eqs. (50) by first

putting them in a more suitable form.

Addition and subtraction of Eqs. (50a) and (50b) gives

$$\int_{-\infty}^{\infty} \left(\frac{1}{\sqrt{1-\lambda^2}} + \eta_1\right) \left[Q_{1e}(\lambda)(1 + e^{-j2k\ell\sqrt{1-\lambda^2}}) + Q_{2m}(\lambda)(1 - 3^{-2jk\ell\sqrt{1-\lambda^2}}\right]$$

$$\cdot\, e^{-jkx\lambda}\, d\lambda = -\left[\left(1 + e^{-2jk\ell\sqrt{1-\lambda_0^2}}\right) - \eta_1\sqrt{1 - \lambda_0^2}\left(1 - e^{-2jk\ell\sqrt{1-\lambda_0^2}}\right)\right]e^{jkx\lambda_0}$$

and

$$\int_{-\infty}^{\infty} \left(\frac{1}{\sqrt{1 - \lambda^2}} + \eta_1 \right) \left[Q_{2e}(\lambda)(1 - e^{-2jk\ell\sqrt{1-\lambda^2}}) + Q_{1m}(\lambda)(1 + e^{-2jk\ell\sqrt{1-\lambda^2}}) \right]$$

$$\cdot e^{-jkx\lambda} \, d\lambda = -\left[(1 - e^{-2jk\ell\sqrt{1-\lambda_0^2}}) - \eta_1 \sqrt{1 - \lambda_0^2} (1 + e^{-2jk\ell\sqrt{1-\lambda_0}}) \right] e^{jkx\lambda_0}$$

$$\tag{51b}$$

where $x > 0$,

$$Q_{1e}(\lambda) = P_{1e}(\lambda) + P_{2e}(\lambda) = U_{1e}(\lambda) + U_{2e}(\lambda) \quad, \tag{52a}$$

$$Q_{1m}(\lambda) = P_{1m}(\lambda) + P_{2m}(\lambda) = \sqrt{1 + \lambda} \, [U_{1m}(\lambda) + U_{2m}(\lambda)] \quad, \tag{52b}$$

$$Q_{2e}(\lambda) = P_{1e}(\lambda) - P_{2e}(\lambda) = U_{1e}(\lambda) - U_{2e}(\lambda) \quad, \tag{52c}$$

and

$$Q_{2m}(\lambda) = P_{1m}(\lambda) - P_{2m}(\lambda) = \sqrt{1 + \lambda} \, [U_{1m}(\lambda) - U_{2m}(\lambda)] \quad. \tag{52d}$$

Clearly, according to (52), $Q_{1e}(\lambda)$ and $Q_{2e}(\lambda)$ are U-functions. It is also important to note that $Q_{\substack{1e \\ 2e}}(\lambda)$ are associated with the electric current spectra while $Q_{\substack{1m \\ 2m}}(\lambda)$ are associated with the magnetic current spectra. Thus, $Q_{1m}(\lambda)$ and $Q_{2m}(\lambda)$ must vanish when $\eta_1 = 0$ (perfectly conducting half planes). Based on this observation and reciprocity considerations, it is concluded that Eqs. (51) are equivalent to the following four equations:

$$\int_{-\infty}^{\infty} \left(\frac{1}{\sqrt{1 - \lambda^2}} + \eta_1 \right) Q_{1e}(\lambda)(1 + e^{-2jk\ell\sqrt{1-\lambda^2}}) d\lambda = -(1 + e^{-j2k\ell\sqrt{1-\lambda_0^2}}) e^{jkx\lambda_0} \quad ,$$

$$\int_{-\infty}^{\infty} \left(\frac{1}{\sqrt{1 - \lambda^2}} + \eta_1 \right) Q_{1m}(\lambda)(1 + e^{-jk\ell\sqrt{1-\lambda^2}}) d\lambda = \eta_1 \sqrt{1 - \lambda_0^2} (1 + e^{-j2k\ell\sqrt{1-\lambda_0^2}}) e^{jkx\lambda_0}$$

$$\int_{-\infty}^{\infty} \left(\frac{1}{\sqrt{1 - \lambda^2}} + \eta_1 \right) Q_{1e}(\lambda)(1 - e^{-j2k\ell\sqrt{1-\lambda^2}}) d\lambda = -(1 - e^{-j2k\ell\sqrt{1-\lambda^2}}) e^{jkx\lambda_0}$$

and

$$\int_{-\infty}^{\infty} \left(\frac{1}{\sqrt{1 - \lambda^2}} + \eta_1 \right) Q_{2m}(\lambda)(1 - e^{-j2k\ell\sqrt{1-\lambda^2}}) d\lambda = \eta_1 \sqrt{1 - \lambda_0^2}(1 - e^{-j2k\ell\sqrt{1-\lambda_0^2}}) e^{jkx\lambda_0}$$

$$(53)$$

for $x > 0$.

We may now close the integration path of (53) by a semi-circle in the lower λ half plane. Subsequently, Cauchy's theorem may be employed to find that (see Chapter II)

$$P_{1e}(\lambda) + P_{2e}(\lambda) = \frac{1}{2\pi j} \frac{L_1(\lambda_0)}{U_1(\lambda)} \frac{U_3(\lambda)U_3(\lambda_0)}{\lambda + \lambda_0} \tag{54a}$$

$$P_{1e}(\lambda) - P_{2e}(\lambda) = \frac{1}{2\pi j} \frac{L_2(\lambda_0)}{U_2(\lambda)} \frac{U_3(\lambda)U_3(\lambda_0)}{\lambda + \lambda_0} \tag{54b}$$

$$P_{1m}(\lambda) + P_{2m}(\lambda) = -\frac{1}{2\pi j} \frac{L_1(\lambda_0)}{U_1(\lambda)} \frac{\eta_1 \sqrt{1 + \lambda_0} \sqrt{1+\lambda} U_3(\lambda)U_3(\lambda_0)}{\lambda + \lambda_0} \tag{54c}$$

$$P_{1m}(\lambda) - P_{2m}(\lambda) = -\frac{1}{2\pi j} \frac{L_2(\lambda_0)}{U_2(\lambda)} \frac{\eta_1 \sqrt{1 + \lambda_0} \sqrt{1+\lambda} U_3(\lambda)U_3(\lambda_0)}{\lambda + \lambda_0} \tag{54d}$$

The split function $U_{1,2}(\lambda)$ and $L_{1,2}(\lambda)$ are the same as those in Eqs. (13) and are given in Appendix I. In addition, $U_3(\lambda)$ is another split function which also occurs in the solution of the diffraction by a single impedance half plane. It is found according to

$$\left(\frac{1}{\sqrt{1-\lambda^2}} + \eta_1\right)^{-1} = U_3(\lambda;\eta_1)L_3(\lambda;\eta_1) \quad , \tag{55}$$

where $L_3(-\lambda;\eta_1) = U_3(\lambda;\eta_1)$. Explicit non-integral expressions of $U_3(\lambda)$ for the $e^{j\omega t}$ time convention are given in Appendix II. These were originally obtained by Senior [10] and approximate non-integral expressions can be found in [11].

From (54) we finally obtain that

$$P_{\substack{1e \\ 2e}}(\cos \phi) = \frac{1}{4\pi j} \frac{U_3(\cos \phi;\eta_1)U_3(\cos \phi_0;\eta_1)}{\cos \phi + \cos \phi_0} \left[\frac{L_1(\cos \phi_0)}{U_1(\cos \phi)} \pm \frac{L_2(\cos \phi_0)}{U_2(\cos \phi)}\right]$$

$$\tag{56a}$$

and

$$P_{\substack{1m \\ 2m}}(\sin \phi) = \frac{1}{4\pi j} \frac{2\eta_1 \cos \phi/2 \cos \phi_0/2}{\cos \phi + \cos \phi_0} U_3(\cos \phi;\eta_1)U_3(\cos \phi_0;\eta_1)$$

$$\cdot \left[\frac{L_1(\cos \phi_0)}{U_1(\cos \phi)} \pm \frac{L_2(\cos \phi_0)}{U_2(\cos \phi)}\right] \quad . \tag{56b}$$

Substituting (56) into (43) and (42), it is found that an asymptotic expression for the scattered field is

$$E_z^{sb} \sim D_s^I(\phi,\phi_0;\eta_1)A(\phi,\phi_0;\ell) \frac{e^{-jkr}}{\sqrt{r}} \quad . \tag{57}$$

$\Delta(\phi,\phi_0,\ell)$ is again given by (22) and $D_s^I(\phi,\phi_0;\eta_1)$ is the diffraction coefficients for the edge of an impedance half plane given by

$$D_s^I(\phi,\phi_0;\eta_1) = \frac{e^{-j\pi/4}}{\sqrt{2\pi k}} \frac{1 - 2\eta_1 \cos \phi/2 \cos \phi_0/2}{\cos \phi + \cos \phi_0} U_3(\cos \phi;\eta_1)U_3(\cos \phi_0;\eta_1)$$

(58)

When $\eta_1 \to 0$ we find from the expressions in Appendix II that

$$U_3(\cos \phi;\eta_1)\big|_{\eta\to0} = \sqrt{2} \sin \phi/2$$

(59)

and thus Eqs. (57) and (58) reduces to Eqs. (32) and (33), respectively. This was to be expected.

3.4 H_z Incidence

The scattered field associated with the H_z incidence on the pair of impedance half planes in Fig. 1(b) requires the use of Eqs. (45) and (46) and to follow the procedure outlined for the E_z incidence. As seen, this is a rather tedious process. However, this is not necessary since we may invoke the principle of duality and obtain that

$$H_z^{sb} \sim D_h^I(\phi,\phi_0;\eta_1)\Delta(\phi,\phi_0;\ell) \frac{e^{-jkr}}{\sqrt{r}}$$

(60)

where

$$D_h^I(\phi,\phi_0;\eta_1) = D_s^I(\phi,\phi_0;1/\eta_1) \quad .$$

(61)

Again, when $\eta_1 \to 0$, the diffraction coefficient D_h^I should reduce to that in (20). Indeed, we note that

$$U_3(\cos \phi;1/\eta_1)\big|_{\eta_1\to0} \to \sqrt{\eta_1}$$

(62)

and from (58) and (61) it is clear that the solution in (60) reduces to (19) or (21).

3.5 A GTD Solution for Large ℓ

Similarly to the perfectly conducting geometry in Fig. 1(a) we may also obtain a GTD solution to the geometry in Fig. 1(b). Equation (35) is still valid, however, all of the diffraction components in (34) must be modified to include the dependence on the surface impedance, η_1. Assuming that the inner walls of the half planes are perfectly conducting, it is relatively easy to see that these take the form,

$$u_z^1 = D_{\substack{s \\ h}}^I(\phi,\phi_0;\eta_1) \frac{e^{-jkr}}{\sqrt{r}} \ , \tag{63a}$$

$$u_z^2 = D_{\substack{s \\ h}}^I(\phi,\phi_0;\eta_1)e^{-j2k\ell(\sin \phi + \sin \phi_0)} \frac{e^{-jkr}}{\sqrt{r}} \ , \tag{63b}$$

$$u_z^{12} = \frac{e^{-j\pi/4}}{\sqrt{4\pi k\ell}} \left(\frac{1}{\cos \phi} + \frac{1}{\cos \phi_0} \right) D_{\substack{s \\ h}}^I(\phi,\phi;\eta_1)e^{-j2k\ell \sin \phi_0}$$

$$\cdot \left[\sum_{m=0}^{\infty} (\Gamma_0)^{2m} \frac{e^{-j(2m+1)2k\ell}}{(2m + 1)^{3/2}} \right] \frac{e^{-jkr}}{\sqrt{r}} \tag{63c}$$

$$u_z^{21} = \frac{e^{-j\pi/4}}{\sqrt{4\pi k\ell}} \left(\frac{1}{\cos \phi} + \frac{1}{\cos \phi_0} \right) D_{\substack{s \\ h}}^I(\phi,\phi_0;\eta_1)e^{-jk\ell \sin \phi}$$

$$\cdot \left[\sum_{m=0}^{\infty} (\Gamma_0)^{2m} \frac{e^{-j(2m+1)2k\ell}}{(2m + 1)^{3/2}} \right] \frac{e^{-jkr}}{\sqrt{r}} \ , \tag{63d}$$

$$u_z^{11} = \frac{e^{-j\pi/4}}{\sqrt{4\pi k\ell}} \left(\frac{1}{\cos\phi} + \frac{1}{\cos\phi_0}\right) D_{\substack{s\\h}}^{I}(\phi,\phi_0;\eta_1)$$

$$\cdot \left[\sum_{m=1}^{\infty} (\Gamma_0)^m \frac{e^{-j(2m)2k\ell}}{(2m)^{3/2}}\right] \frac{e^{-jkr}}{\sqrt{r}} \quad , \tag{63e}$$

and

$$u_z^{22} = \frac{e^{-j\pi/4}}{\sqrt{4\pi k\ell}} \left(\frac{1}{\cos\phi} + \frac{1}{\cos\phi_0}\right) D_{\substack{s\\h}}^{I}(\phi,\phi_0;\eta_1)e^{-j2k\ell(\sin\phi + \sin\phi_0)}$$

$$\cdot \left[\sum_{m=1}^{\infty} (\Gamma_0)^m \frac{e^{-j(2m)2k\ell}}{(2m)^{3/2}}\right] \frac{e^{-jkr}}{\sqrt{r}} \tag{63f}$$

where

$$\Gamma_0 = \pm 1 \ . \tag{64}$$

Clearly, this factor stems from the multiple reflections between the

half planes. As mentioned in Chapter II, only two to three interactions

need to be considered for sufficiently accurate results. Again, for

$\ell > 1.5 \ \lambda$ the scattered field can be safely approximated by

$$\left.\begin{array}{c} E_z^{sb}\\ \\ H_z^{sb} \end{array}\right\} \sim D_{\substack{s\\h}}^{I}(\phi,\phi_0;\eta_1) \ \cos[k\ell(\sin\phi + \sin\phi_0)] \ e^{-jk\ell(\sin\phi + \sin\phi_0)} \frac{e^{-jkr}}{\sqrt{r}} \ .$$

$$\tag{65}$$

IV. DIFFRACTION BY AN IMPEDANCE HALF PLANE IN THE PRESENCE OF A GROUND OR IMPEDANCE PLANE

4.1 Diffraction by an Impedance Half Plane in the Presence of a Ground Plane

The solution of the diffracted field by the geometry in Fig. 1(c) can be obtained from the respective solution by the geometry in Fig. 1(b) via image theory. In particular, as shown in Fig. 4, the problem of diffraction by the geometry in Fig. 1(c) is equivalent to the sum of two diffracted fields from a pair of parallel impedance half planes. One of the diffracted fields is due to the direct wave and the other is due to an image wave. If the incident wave is given by

$$u_z^i = \left\{ \begin{matrix} E_z^i \\ H_z^i \end{matrix} \right\} = e^{+jk(x \cos \phi_0 + y \sin \phi_0)} , \quad (66)$$

the image wave satisfying the necessary boundary conditions on the ground plane is

$$u_z^I = \left\{ \begin{matrix} E_z^I \\ H_z^I \end{matrix} \right\} = {}^-_+ e^{jk(x \cos \phi_I + y \sin \phi_I)} e^{-j2k\ell \sin \phi_0} \quad (67)$$

where

$$\phi_I = 2\pi - \phi_0 . \quad (68)$$

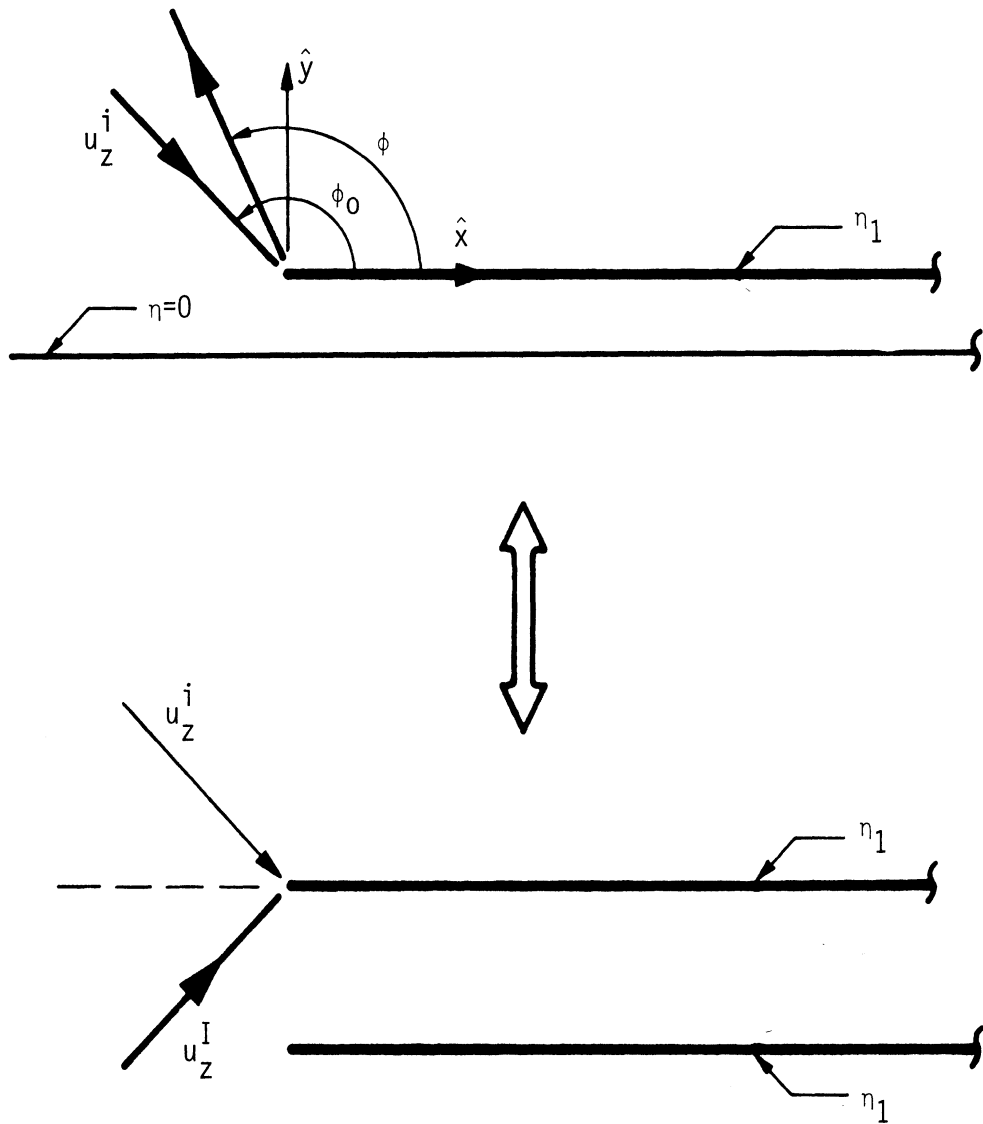The diffracted field due to a plane wave incident on the geometry of Fig. 1(c) is now expressed by

Figure 4.   Illustration of the application of image
theory to the problem of diffraction by the
geometry in Fig. 1(c).

$$E_z^{sc}(\phi,\phi_0) = E_z^{sb}(\phi,\phi_0) - E_z^{sb}(\phi,2\pi - \phi_0)e^{-2jk\ell \sin \phi_0} \qquad (69a)$$

for the E_z-incidence and by

$$H_z^{sc}(\phi,\phi_0) = H_z^{sb}(\phi,\phi_0) + H_z^{sb}(\phi,2\pi - \phi_0)e^{-2jk\ell \sin \phi_0} \qquad (69b)$$

in case of the H_z-incidence. $E_z^{sb}(\phi,\phi_0)$ and $H_z^{sb}(\phi,\phi_0)$ are the scattered fields associated with the geometry in Fig. 1(b) and are given by Eqs. (57) and (60), respectively. In addition, $E_z^{sb}(\phi, 2\pi - \phi_0)$ and $H_z^{sb}(\phi,2\pi - \phi_0)$ are given by the same expressions provided the incidence angle is set to $2\pi - \phi_0$ instead of the usual ϕ_0. We further note that the GTD expression for E_z^{sb} and H_z^{sb} is Section 5 of Chapter III may be used in (69) whenever applicable.

4.2 Diffraction by an Impedance Half Plane in the Presence of an Impedance Plane

The geometry corresponding to this problem is shown in Fig. 1(d). This is already the same geometry as that in Fig. 1(c) when $\eta_2 = 0$. The diffracted field by the structure in Fig. 1(c) was obtained in the previous section after invoking image theory and in connection with the solution for the diffraction by the geometry in Fig. 1(b). A similar formulation can then be used for obtaining the diffracted field by the structure in Fig. 1(d). However, in this case a more detailed analysis is required in order to determine the extent of the application of image theory when the ground plane is replaced by an impedance plane.

Figure 5 depicts the 12 actual diffraction mechanisms that exist in relation to the geometry in Fig. 1(d) and their equivalent when

the geometry is replaced with that in Fig. 1(b) which consists of two parallel impedance half planes. Figure 5(a) illustrates the scattering mechanisms associated with the direct field or equivalent along the direction of incidence and Fig. 5(b) those simulated by an equivalent image field. The factor appearing by the equivalent incident rays must multiply the scattered field produced by that mechanism in order to fully simulate the actual one. These factors are basically the plane wave reflection coefficients for an impedance plane as a function of the angle of incidence. More precisely,

$$
\Gamma(\phi) = \begin{cases} \Gamma_s(\phi) = \dfrac{\eta_1 \sin \phi - 1}{\eta_1 \sin \phi + 1} \\[4mm] \Gamma_h(\phi) = \dfrac{\eta_1 - \sin \phi}{\eta_1 + \sin \phi} \end{cases}
\tag{70}
$$

which reduces to Γ_0 in Eq. (64) when $\phi = \pi/2$. Note that $\Gamma_s(\phi)$ refers to the E_z incidence while $\Gamma_h(\phi)$ refers to the H_z-incidence.

Based on our previous GTD analyses (see Fig. 3) given in Section 2.4 and 3.5, it is now a relatively simple task to develop a similar GTD solution for the diffracted fields associated with the mechanisms in Fig. 5. As before (see Eq. (35)), the total diffracted field for large ℓ is given by

$$
u_d^{sd} = \begin{Bmatrix} E_z^{sd} \\[4mm] H_z^{sd} \end{Bmatrix} \sim u_z^1 + u_z^2 + u_z^{12} + u_z^{21} + u_z^{11} + u_z^{22}
$$

$$
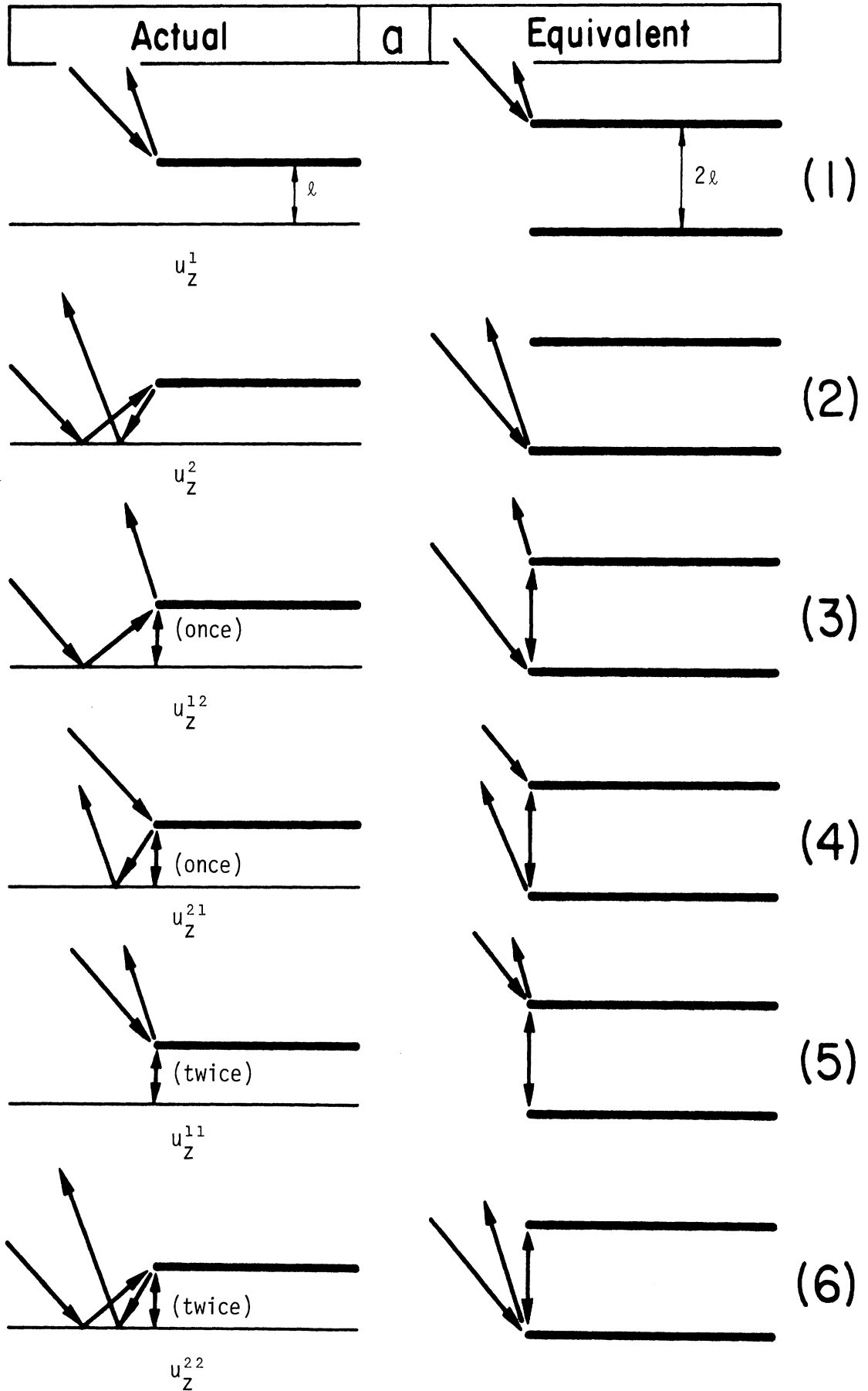+ (u_{zI}^1 + u_{zI}^2 + u_{zI}^{12} + u_{zI}^{21} + u_{zI}^{11} + u_{zI}^{22})e^{-2jk\ell \sin \phi_0}
$$

$$
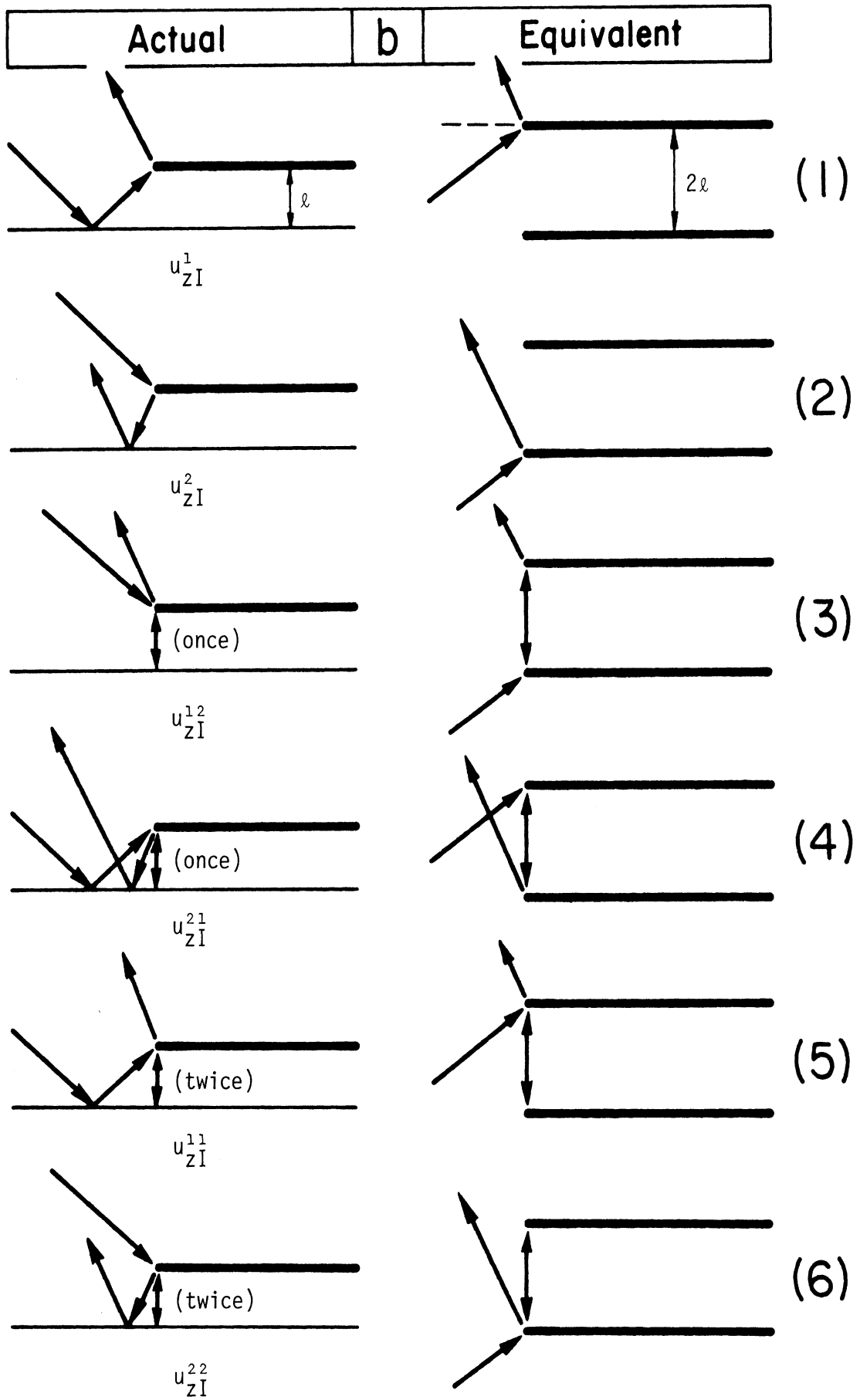\tag{71}
$$

Figure 5. Actual mechanisms for the structure in
Figure 1(d) and their equivalent.

Actual	b	Equivalent

u_{zI}^1 ℓ 2ℓ (1)

u_{zI}^2 (2)

u_{zI}^{12} (once)   (3)

u_{zI}^{21} (once)   (4)

u_{zI}^{11} (twice)   (5)

u_{zI}^{22} (twice)   (6)

where the components with the subscript I refer to the image

mechanisms.

From Fig. 5(a) we observe that u_z^1 is the same as in (63a). In

addition

$$u_z^2 = \Gamma_{s_h}(\phi_0)\Gamma_{s_h}(\phi)\ u_z^{2b} \ , \tag{72a}$$

$$u_z^{12} = \Gamma_{s_h}(\phi_0)\Gamma_0\ u_z^{12b} \ , \tag{72b}$$

$$u_z^{21} = \Gamma_{s_h}(\phi)\Gamma_0\ u^{21b} \ , \tag{72c}$$

$$u_z^{11} = (\Gamma_0)^2\ u_z^{11b} \tag{72d}$$

and

$$u_z^{22} = \Gamma_{s_h}(\phi_0)\Gamma_{s_h}(\phi)(\Gamma_0)^2\ u_z^{22b} \ , \tag{72e}$$

where the superscript b indicates components corresponding to the

structure in Fig. 1(b) and are given in (63).

The components associated with the image mechanisms in Fig. 5(b)

can be expressed in a similar manner as follows:

$$u_{zI}^1 = \Gamma_{s_h}(\phi_0)u_z^{1b}(\phi,\phi_I) \ , \tag{73a}$$

$$u_{zI}^2 = \Gamma_{s_h}(\phi)u_z^{2b}(\phi,\phi_I) \ , \tag{73b}$$

$$u_{zI}^{12} = \Gamma_0\ u_z^{12b}(\phi,\phi_I) \ , \tag{73c}$$

$$u_{zI}^{21} = \Gamma_{s_h}(\phi)\Gamma_{s_h}(\phi_0)\Gamma_0\ u_z^{21b}(\phi,\phi_I) \ , \tag{73d}$$

$$u_{zI}^{11} = \Gamma_s(\phi_0)(\Gamma_0)^2 \; u_z^{11b}(\phi,\phi_I) \quad , \tag{73e}$$

$$u_{zI}^{22} = \Gamma_s(\phi)(\Gamma_0)^2 \; u_z^{22b}(\phi,\phi_I) \tag{73f}$$

and $u_z^{jb}(\phi,\phi_I)$ are again found from Eqs. (63) provided ϕ_0 is replaced

by $\phi_I = 2\pi - \phi_0$.

The above GTD solution is only valid for large ℓ. However,

when ℓ is small the field associated with the multiple interactions cannot

be considered optical and we must then develop a solution in terms of

the expressions given in Eqs. (57) and (60) as done in the previous

section. Unfortunately, an exact solution is not possible since the

ray mechanisms in Figs. 5(a) and 5(b) (see also Eqs. (72) and (73)) are not

all multiplied by the same factor. Thus, an approximate solution will

suffice at this point. It is important, though, that the contribution

of the first order terms, u_z^1, u_z^2, u_{zI}^1 and u_{zI}^2 be calculated correctly since

these dominate the total diffracted field. Fortunately, this can be

accomplished by rewriting the diffracted field corresponding to the

structure in Fig. 1(b) in a more convenient form.

In particular, Eqs. (57) and (60) can be written as follows:

$$\left. \begin{array}{c} E_z^{sb} \\ \\ H_z^{sb} \end{array} \right\} = \left\{ \begin{array}{c} E_{1z}^{sb} + E_{2z}^{sb} \\ \\ H_{1z}^{sb} + H_{2z}^{sb} \end{array} \right. \quad . \tag{74}$$

The components with subscript 1 correspond to the total diffracted

field by the top impedance half plane and those with subscript 2 to the

diffracted field by the bottom impedance half plane. Note that the

total diffracted field, for example, by the top half plane includes the components u_z^1, u_z^{12}, and u_z^{11}. From Eqs. (56) and (43), this diffracted field is given by

$$
\left.\begin{array}{c} E^{sb}_z \\[2mm] H^{sb}_z \end{array}\right\} = D^I_{\substack{s \\ h}}(\phi,\phi_0;n_1)\Delta_+(\phi,\phi_0;\ell)\ \frac{e^{-jkr}}{\sqrt{r}}
$$

$$
= \left\{ D^I_{\substack{s \\ h}}(\phi,\phi_0;n_1) + D^I_{\substack{s \\ h}}(\phi,\phi_0;n_1)\ [\Delta_+(\phi,\phi_0;\ell) - 1]\right\} \frac{e^{-jkr}}{r} \qquad (75)
$$

and thus the contribution of u_z^1 is now explicit. Similarly, for the diffracted field by the bottom half plane we have

$$
\left.\begin{array}{c} E^{sb}_{2z} \\[2mm] H^{sb}_{2z} \end{array}\right\} = \left\{ D^I_{\substack{s \\ h}}(\phi,\phi_0;n_1)\ e^{-j2k\ell \sin \phi_0} + D^I_{\substack{s \\ h}}(\phi,\phi_0;n_1)[\Delta_-(\phi,\phi_0;\ell) \right.
$$
$$
\left. - e^{-j2k\ell \sin \phi_0}]\right\} e^{-j2k\ell \sin\phi}\ \frac{e^{-jkr}}{\sqrt{r}} \ . \qquad (76)
$$

The functions $\Delta_\pm(\phi,\phi_0;\ell)$ are defined by

$$
\Delta_\pm(\phi,\phi_0,\ell) = \frac{1}{2}\left[\frac{L_1(\cos \phi_0)}{U_1(\cos \phi)} \pm \frac{L_2(\cos \phi_0)}{U_2(\cos \phi)} \right] \qquad (77)
$$

and $D^I_{\substack{s \\ h}}(\phi,\phi_0;n_1)$ is given in (58).

We may now construct an approximate solution for the diffracted field by the structure in Fig. 1(d). Looking at Fig. 5, we have that for small ℓ (less than one wavelength)

$$
u^{sd}_z = \left.\begin{array}{c} E^{sd}_z \\[2mm] H^{sd}_z \end{array}\right\} = u^{top}_z + u^{bot}_z + \left(u^{top}_{zI} + u^{bot}_{zI}\right)e^{-2jk\ell \sin\phi_0}
$$
$$
\qquad (78)
$$

where

$$u_z^{top} \cong \left\{ D_{s \atop h}^I(\phi,\phi_0;n_1) + \Gamma(\phi_0)\Gamma_0 \; D_{s \atop h}^I(\phi,\phi_0;n_1)[\Delta_+(\phi,\phi_0;\ell) - 1] \right\} \frac{e^{-jkr}}{\sqrt{r}} ,$$

(79a)

$$u_{zI}^{top} \cong \left\{ \Gamma_{s \atop h}(\phi_0)D_{s \atop h}^I(\phi,\phi_I;n_1) + \Gamma_0 \; D_{s \atop h}^I(\phi,\phi_I;n_1)[\Delta_+(\phi,\phi_I;\ell) - 1] \right\} \frac{e^{-jkr}}{\sqrt{r}} ,$$

(79b)

$$u_z^{bot} \cong \left\{ \Gamma_{s \atop h}(\phi)\Gamma_{s \atop h}(\phi_0)D_{s \atop h}^I(\phi,\phi_0;n_1)e^{-j2k\ell \sin \phi_0} + \Gamma_{s \atop h}(\phi)\Gamma_0 \; D_{s \atop h}^I(\phi,\phi_0;n_1) \right.$$

$$\left. [\Delta_-(\phi,\phi_0;\ell) - e^{-j2k\ell \sin \phi_0}] \right\} e^{-j2k\ell \sin \phi} \frac{e^{-jkr}}{\sqrt{r}}$$

(79c)

and

$$u_{zI}^{bot} \cong \left\{ \Gamma_{s \atop h}(\phi)D_{s \atop h}^I(\phi,\phi_I;n_1)e^{j2k\ell \sin \phi_0} + \Gamma_{s \atop h}(\phi)\Gamma_{s \atop h}(\phi_0)\Gamma_0 \; D_{s \atop h}(\phi,\phi_I;n_1) \right.$$

$$\left. [\Delta_-(\phi,\phi_I;\ell) - e^{j2k\ell \sin \phi_0}] \right\} e^{-j2k\ell \sin \phi} \frac{e^{-jkr}}{\sqrt{r}} .$$

(79d)

The above take into consideration that backscattering is of primary interest here. We further note that they are rather conservative approximations and thus they would most likely give a higher result than the correct one. This is true provided $|\Gamma_0| < 1$ as usual. In fact, the smaller the value of $|\Gamma_0|$ or $|\Gamma_{s \atop h}|$, the better the approximation in (79) become. For this case only the dominant terms of (79) need to be considered. These are the first terms from each of the expressions (79a) through (79d).

V. CONCLUSIONS AND FUTURE STUDIES

In this study we presented rigorous solutions to the problems of diffraction for the first three configurations in Fig. 5. The diffraction by the last geometry in Fig. 5 was considered only in an approximate manner. Further, the configurations in Fig. 1(c) and 1(d) were based on the rigorous solution to the diffraction by two parallel impedance half planes. The last was obtained via a generalization of the angular spectrum method to account for the concurrent existence of both electric and magnetic currents.

The above results can be readily used and extended to the analysis of a small step discontinuity or a protrusion associated with impedance boundary conditions as shown in Fig. 6(a). This will involve the study of the scattering by a parallel plate waveguide with a recessed stub as shown in Fig. 6(b). For $d \to 0$, the configuration in Fig. 6(b) reduces to that in 6(a). In case of E_z incidence and $\ell < \lambda/4$, the dominant diffraction emanates from the edges only and thus the effect of the stub can be totally neglected. Consequently, the analysis in this report is sufficient for the step discontinuities provided $\ell < \lambda/4$.

For the H_z incidence, the diffraction by the waveguide edge is negligible when ϕ and ϕ_0 are near 180 degrees, but there exists a strong coupling into waveguide modes. Thus, the scattering due to the presence of the stub will be dominant in that region. Again, assuming that $\ell < \lambda$, only the TEM mode will be non-decaying. Subsequently, once the coupling coefficient, $C_0(\phi)$, the reflection coefficient, R_0
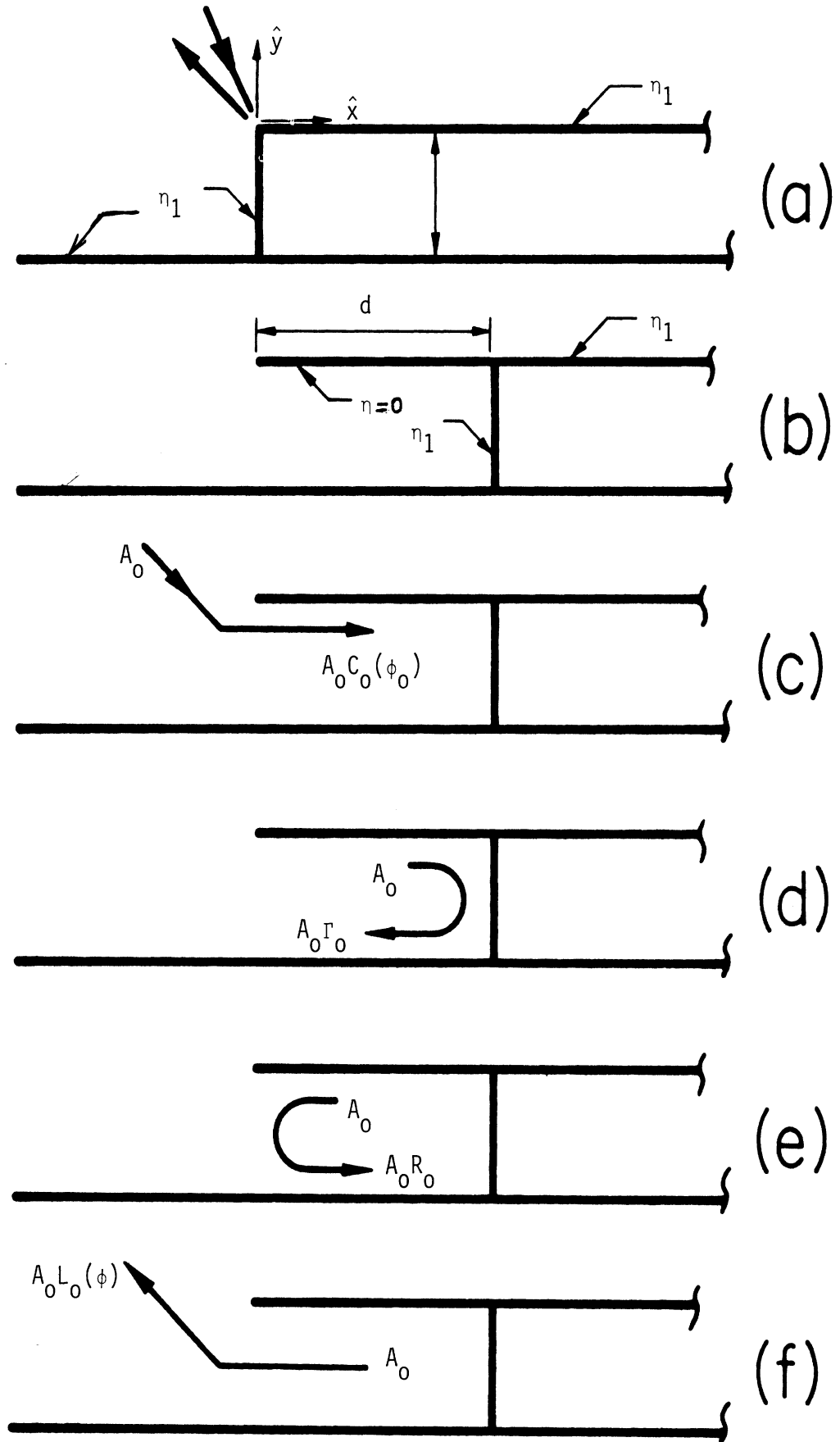
Figure 6. (a) Geometry of a protrusion
(b) Geometry to be analyzed
(c) - (f) Illustration of coupling
reflection and launching mechanisms

and the launching coefficient, $L_0(\phi)$, are found (see Fig. 6), the scattered field can be expressed as [5]

$$H_z^s = P(\phi,\phi_0) \frac{e^{-j\pi/4}}{\sqrt{2\pi k}} \frac{e^{-jkr}}{\sqrt{r}}$$

where

$$P(\phi,\phi_0) = S(\phi,\phi_0) + \frac{L_0(\phi)C_0(\phi_0)\Gamma_0}{1 - R_0\Gamma_0}.$$

In the above $S(\phi,\phi_0)$ is the diffraction pattern of the waveguide edges and can be extracted from Eqs. (21) or (60). Further Γ_0 is the plane wave reflection coefficient given in (64).

APPENDIX I. DEFINITION OF THE SPLIT FUNCTIONS $U_1(\lambda)$ AND $U_2(\lambda)$

We wish to factorize the functions $(1 \pm e^{-j2k\ell\sqrt{1-\lambda^2}})$ such that (see also Eqs. (13))

$$1 + e^{-j2k\ell\sqrt{1-\lambda^2}} = U_1(\lambda)L_1(\lambda) \qquad (A.1)$$

and

$$1 - e^{-j2k\ell\sqrt{1-\lambda^2}} = U_2(\lambda)L_2(\lambda) \ . \qquad (A.2)$$

The U-functions are regular in the upper λ-half plane shown in Fig. A.2 and the L-functions have similar properties in the lower λ-half plane.

Assuming an $e^{j\omega t}$ time dependence and following the procedure in [6] we find that $U_1(\lambda)$ is given by

$$U_1(\lambda) = L_1(-\lambda) = \sqrt{2} \exp[-X_1(\lambda) - T(\lambda)] \prod_{n=1,3,5}^{\infty} \left(-\frac{2j\ell}{n\pi}\right)(k\lambda + j\gamma_n)e^{j2k\ell\lambda/n\pi}$$

$$\qquad (A.3)$$

where

$$X_1(\lambda) = -\frac{jk\lambda\ell}{\pi}\left[1 - C + \ln\left(\frac{\pi}{2k\ell}\right)\right] - \frac{k\ell\lambda}{2} \qquad (A.4)$$

$$T(\lambda) = \frac{\ell\gamma}{\pi}\begin{cases} \pi - \cos^{-1}(\lambda) & \lambda > 0 \\ \cos^{-1}(-\lambda) & \lambda < 0 \end{cases} \qquad (A.5)$$

$$\gamma = \begin{cases} k\sqrt{\lambda^2 - 1} \ , \text{ or} \\ jk\sqrt{1 - \lambda^2} \ , \end{cases} \qquad (A.6)$$

$$\gamma_n = \begin{cases} k\sqrt{\left(\frac{n\pi}{2k}\right)^2 - 1} & , \text{ or} \\ jk\sqrt{1 - \left(\frac{n\pi}{2k\ell}\right)^2} & \end{cases} \qquad (A.7)$$

and

$$C = 0.5772 \ . \qquad (A.8)$$

Note that $X_1(\lambda)$ was chosen such that $U_1(\lambda)$ is asymptotic to a constant as $|\lambda| \to \infty$.

Similarly we find that

$$U_2(\lambda) = L_2(-\lambda) = e^{j\pi/4} \sqrt{2k\ell}\sqrt{1 - \lambda} \ \exp[-X_2(\lambda) - T(\lambda)] \prod_{n=2,4,6}^{\infty}$$

$$\cdot \left(- \frac{2j\ell}{n\pi}\right)(k\lambda + j\gamma_n)e^{j2k\ell\lambda/n\pi} \ , \qquad (A.9)$$

where

$$X_2(\lambda) = - \frac{jk\ell\lambda}{\pi}\left[1 - C + \ln\left(\frac{2\pi}{k\ell}\right)\right] - \frac{k\ell\lambda}{2} \qquad (A.10)$$

and all other functions and parameters were defined in (A.5) through (A.8).

The above expressions for $U_{1,2}(\lambda)$ appear cumbersome because they consist of infinite homomorphic products. However, for our intended calculations where $\ell < \lambda/4$, we find that the achieved amplitude accuracy is within five percent by retaining only the first three terms of the product series. Further, the accuracy is improved for smaller ℓ. Note that 2ℓ is the separation distance between the two half planes shown in Fig. 1(a).

APPENDIX II.   DEFINITION OF THE SPLIT FUNCTION $U_3(\lambda)$

The function

$$F(\lambda;\eta) = \left(\frac{1}{\sqrt{1 - \lambda^2}} + \eta \right)^{-1} \tag{B.1}$$

occurs in the solution of the problem of diffraction by an impedance

half plane or by a set of parallel half planes as discussed in

Chapter III.   To obtain the final form of the solution to the above

problems, it is first required that the function in (B.1) be factorized

in the form (see also Eq. (55))

$$\left(\frac{1}{\sqrt{1 - \lambda^2}} + \eta \right)^{-1} = U_3(\lambda;\eta)L_3(\lambda;\eta) \quad . \tag{B.2}$$

As usual $U_3(\lambda;\eta)$ is regular in the upper λ-half plane shown in Fig. A.2

and $L_3(\lambda;\eta)$ has the same property in the lower λ-half plane.

Expressions for $U_3(\lambda;\eta) = L_3(-\lambda;\eta)$ are given by Senior [10] in

an integral form and approximate explicit ones were later found by

Volakis and Senior [12]. We simply state below the results in [10] and

[11]. Assuming an $e^{j\omega t}$ time dependence we have that

$$U_3(\lambda = \cos \phi;\eta) = \frac{2[2 \cos \chi(1 - \cos \phi)]^{1/2}}{\left(\sqrt{2} \sin \frac{\phi - \chi}{2} + 1 \right)\left(\sqrt{2} \sin \frac{\phi + \chi}{2} + 1 \right)}$$
$$\cdot \left\{ \frac{\psi_\pi(\pi-\phi+\chi)\psi_\pi(\pi-\phi-\chi)}{\psi_\pi(\pi/2) \; \psi_\pi(\pi/2)} \right\}^2 \quad , \tag{B.3}$$

where

$$\cos \chi = 1/n \tag{B.4}$$

and $\psi_\pi(\alpha)$ is the Maliuzhinets [12] function given by

$$\psi_\pi(\alpha) = \exp\left\{-\frac{1}{8\pi} \int_0^\alpha \frac{\pi \sin u - 2\sqrt{2} \pi \sin u/2 + 2u}{\cos u} \, du\right\}$$

$$\approx \begin{cases} 1 - 0.0139 \, \lambda^2 \, , & 0 \leq \sigma \leq \pi/2 \, , \quad \tau \leq 4.6 \\[3em] 1.05302 \, [\cos 1/4(\alpha - j\gamma_0)]^{1/2} \, \exp \frac{j\alpha}{2} \, e^{j\alpha} \, , & 0 \leq \sigma \leq \pi/2 \, , \quad \tau > 4.6 \end{cases}$$

$$\tag{B.5}$$

with $\alpha = \sigma + j\tau$ and $\gamma_0 = 0.69315$. For other values of σ, the identity

$$\psi_\pi(\alpha) = 0.93242 \, \frac{\cos\left(\frac{\alpha}{4} - \frac{\pi}{8}\right)}{\psi_\pi(\alpha - \pi)}$$

may be employed as many times as required before the approximation in (B.5) can be used. It is shown in [12] that this approximation gives a maximum amplitude error of 0.27 percent and a corresponding phase error of 2.4 percent.

References

[1] A. E. Heins, "The reflection of electromagnetic waves by an infinite set of plates III," Quart. Appl. Math. 8, pp. 281-291, 1950.

[2] A. E. Heins and J. F. Carlson, "The reflection of electromagnetic waves by an infinite set of plates II," Quart. Appl. Math. 5, pp. 82-88, 1947.

[3] P. C. Clemmow, "A method for the exact solution of a class of two dimensional diffraction problems," Proc. Royal Soc. A (205), pp. 286-308, 1951.

[4] P. C. Clemmow, The Plane Wave Spectrum Representation of Electro-magnetic Fields, Pergamon Press, 1966.

[5] S-W Lee and R. Mittra, "Diffraction by thick conducting half plane and a dielectric-loaded waveguide," IEEE Trans. on Antennas and Propagat., AP-16, No. 4, pp. 454-461, July 1967.

[6] B. Noble, Methods Based on the Weiner-Hopf Technique, Pergamon Press, 1958.

[7] R. G. Kouyoumjian and P. H. Pathak, "A uniform geometrical theory of diffraction for an edge in a perfectly conducting surface," Proc. IEEE, Vol. 62, No. 11, pp. 1448-1461, November 1974.

[8] J. J. Bowman, "Comparison of ray theory with exact theory for scattering by open waveguides," SIAM J. Appl. Math., Vol. 18, No. 4, pp. 818-829, June 1970.

[9] R. E. Collin, Field Theory of Guided Waves, McGraw-Hill Co., 1960, pp. 461-465.

[10] T.B.A. Senior, "Diffraction by a semi-infinite metallic sheet," Proc. Royal Soc., A, Vol. 213, pp. 436-458, 1952.

[11] J. L. Volakis, "A uniform geometrical theory of diffraction for an imperfectly conducting half plane," submitted for publication to the IEEE Trans. on Antennas and Propagat.

[12] J. L. Volakis and T.B.A. Senior, "Simple expressions for a function occurring in diffraction theory," IEEE Trans. Antennas and Propagat., AP-23, June 1985, pp. 678-680.